SANDIA REPORT

SAND2017-2306 Unlimited Release Printed March 2017

Analysis of Corrosion Residues Collected from the Aluminum Basket Rails of the High-Burnup Demonstration Cask

Charles R. Bryan

Prepared by Sandia National Laboratories Albuquerque, New Mexico 87185 and Livermore, California 94550

Sandia National Laboratories is a multi-mission laboratory managed and operated by Sandia Corporation, a wholly owned subsidiary of Lockheed Martin Corporation, for the U.S. Department of Energy's National Nuclear Security Administration under contract DE-AC04-94AL85000.

Approved for public release; further dissemination unlimited.



Issued by Sandia National Laboratories, operated for the United States Department of Energy by Sandia Corporation.

NOTICE: This report was prepared as an account of work sponsored by an agency of the United States Government. Neither the United States Government, nor any agency thereof, nor any of their employees, nor any of their contractors, subcontractors, or their employees, make any warranty, express or implied, or assume any legal liability or responsibility for the accuracy, completeness, or usefulness of any information, apparatus, product, or process disclosed, or represent that its use would not infringe privately owned rights. Reference herein to any specific commercial product, process, or service by trade name, trademark, manufacturer, or otherwise, does not necessarily constitute or imply its endorsement, recommendation, or favoring by the United States Government, any agency thereof, or any of their contractors or subcontractors. The views and opinions expressed herein do not necessarily state or reflect those of the United States Government, any agency thereof, or any of their contractors.

Printed in the United States of America. This report has been reproduced directly from the best available copy.

Available to DOE and DOE contractors from

U.S. Department of Energy Office of Scientific and Technical Information P.O. Box 62 Oak Ridge, TN 37831

Telephone: (865) 576-8401 Facsimile: (865) 576-5728

E-Mail: reports@adonis.osti.gov
Online ordering: http://www.osti.gov/bridge

Available to the public from

U.S. Department of Commerce National Technical Information Service 5285 Port Royal Rd. Springfield, VA 22161

Telephone: (800) 553-6847 Facsimile: (703) 605-6900

E-Mail: orders@ntis.fedworld.gov

Online order: http://www.ntis.gov/help/ordermethods.asp?loc=7-4-0#online



SAND2017-2306 Unlimited Release Printed March 2017

Analysis of Corrosion Residues Collected from the Aluminum Basket Rails of the High-Burnup Demonstration Cask

Charles R. Bryan
Storage and Transportation Technologies Department
Sandia National Laboratories
P.O. Box 5800
Albuquerque, New Mexico 87185-MS0779

ABSTRACT

On September, 2015, an inspection was performed on the TN-32B cask that will be used for the high-burnup demonstration project. During the survey, wooden cribbing that had been placed within the cask eleven years earlier to prevent shifting of the basket during transport was removed, revealing two areas of residue on the aluminum basket rails, where they had contacted the cribbing. The residue appeared to be a corrosion product, and concerns were raised that similar attack could exist at more difficult-to-inspect locations in the canister. Accordingly, when the canister was reopened, samples of the residue were collected for analysis. This report presents the results of that assessment, which determined that the corrosion was due to the presence of the cribbing. The corrosion was associated with fungal material, and fungal activity likely contributed to an aggressive chemical environment. Once the cask has been cleaned, there will be no risk of further corrosion.

EXECUTIVE SUMMARY

On September 29-30, 2015, a team consisting of Electric Power Research Institute personnel, AREVA personnel (AREVA Federal Services, AREVA TN, and AREVA P&T), and personnel from Dominion Virginia Power performed an inspection of the TN-32B cask that will be used for the high-burnup demonstration project. During the survey, polypropylene-wrapped wooden cribbing that had been placed within the cask over 11 years earlier to prevent shifting of the basket was removed, revealing two small areas of residue on the aluminum basket rails, where they had contacted the cribbing. The nature of the residue was unknown, but it appeared to be a corrosion product and concerns were raised that similar attack could exist at more difficult-to-inspect locations in the canister. The decision was made to collect samples of the residue for evaluation and to allow a technical assessment of the observed attack. This report documents the results of that assessment.

Samples of the suspected corrosion residue were collected the next time the cask was opened (July, 2016) and sent to Sandia National Laboratories (SNL) for analysis. The material sent to SNL consisted of a single bulk sample of the filamentous, spongy residue, and several samples collected by swiping the residues at each of the locations with 5-inch paper filters. At SNL, the samples were imaged and analyzed using a scanning electron microscope (SEM) with an energy dispersive X-ray spectroscopy (EDS) system. Bulk analysis was then carried out using inductively-coupled-plasma mass spectrometry (ICP-MS).

Analysis of the samples showed that aluminum corrosion products were present at both sites. The aluminum-rich material was amorphous aluminum hydroxide; its morphology suggests it formed as a gel. SEM analysis showed that the spongy residue sample was consisted largely of filamentous fungal material. At one of the two sites with deposits, this fungal mat coated the entire corroded region. Embedded within and on the fungal material were grains of the aluminum corrosion product. A brown coating as also present on some of the aluminum hydroxide grains and parts of the fungal mass. Originally suspected of being iron oxide (possibly from corrosion of nails in the cribbing) this material instead appeared to be organic in nature, and SEM EDS analysis showed that it was enriched in potassium, iron, and phosphorous. Also present at each of the two corrosion sites were insect fragments; moreover, dead insects were observed via borescope at the bottom of the cask.

Chemical analysis of the samples showed that many trace metals were present, most of them in amounts consistent with their source being corrosion of Al-6061, the material comprising the basket rails. Elements present in greater amounts than can be explained by corrosion of the aluminum metal were K (the second most abundant metal in the samples), Fe, and P, the species enriched in the organic coating. The brown coating is interpreted to consist of fungal exometabolites and breakdown products of the wood (e.g. organic acids) because fungal exometabolites specifically scavenge and complex important nutrients such as K, Fe, and P from the wood as it is broken down, making them bioavailable to the fungus. The presence of these elements (which must be sourced to the wood), the fungus, and the insect fragments, indicates that the polypropylene wrapping on the cribbing leaked or was was damaged, allowing the wood, or fluids from the wood, to contact the aluminum metal.

The observed attack indicates that an aqueous solution contacted the surface. There are a number of possible explanations for the attack:

- Crevice corrosion
- Corrosion due to chemicals used for wood treatment (a number of which are aggressive with respect to aluminum) leaching out of the cribbing.
- Corrosion due to organic acids leaching out of the wood.
- Corrosion due to alteration of the local chemistry by fungi.

The corrosion could have been due to a combination of crevice effects, organic acids leached from the wood, or fungal growth. Evidence suggests that fungal growth played an important role, possibly through both through direct and indirect processes. Fungal activity produces powerful metal complexants that have been shown to promote aluminum corrosion, but also is the dominant mechanism of wood decay, increasing organic acid release. Regardless of the mechanism, it is clear that corrosion of the aluminum metal was due to contact with the wooden cribbing. Areas not contacted by the cribbing or fluids generated by it are unlikely to be corroded, and once the corroded sites and the cask interior have been thoroughly cleaned (the fluid may have dripped deeper into the cask), further corrosion over the course of the high-burnup demonstration test is unlikely.

ACKNOWLEDGMENTS

This work was carried out with the help of several organizations. The inspection of the high-burnup demonstration cask and sampling of the corrosion residue was carried out by personnel from the Electric Power Research Institute (EPRI), AREVA, and personnel from Dominion Virginia Power, including personnel from the North Anna Nuclear Generating Station. Keith Waldrop of EPRI provided the samples to Sandia for analysis and interpretation. At Sandia, Mark Rodriguez performed XRD analyses, and Jessica Kruichak and Anastasia Ilgen helped with sample preparation and ICP-MS analysis.

CONTENTS

1.	. Introduction		
2.	2. Samples and Methods		
3.	3. Results		
	3.1. SEM/EDS Analysis	21	
	3.2. XRD Analysis	38	
	3.3. Chemical Analysis		
4.	4. Discussion		
5.	5. Conclusions		
6.	5. References		

FIGURES

Figure 1. Photograph of the storage cask, with the lid removed. The locations of the two areas with apparent corrosion residue are shown.	14
Figure 2. Photographs of a) the "debris" on the basket rail (near side), and b) the "residue" on the basket rail (far side)	15
Figure 3. Photographs of high-burnup demonstration cask corrosion samples	18
Figure 4. SEM BSE image of the Debris sample, showing the filamentous fungal matrix and the adhering amorphous aluminum hydroxide.	22
Figure 5. SEM BSE image of the Debris sample, showing the filamentous fungal matrix and the adhering amorphous aluminum hydroxide.	23
Figure 6. SEM BSE images of the Debris sample, showing close-up images of the fungal mat	24
Figure 7. SEM BSE images of the Debris sample, showing the distinctive shrinkage cracks and in some areas, botryoidal morphology of the aluminum hydroxide	25
Figure 8. SEM BSE images of the dry swipe from the debris location, showing the aluminum hydroxide particles adhering to the filter	27
Figure 9. SEM SE image, element mays, and EDS X-ray spectrum of particulates on the surface of the dry swipe from the debris location	28
Figure 10. SEM BSE image of the dry swipe from the residue location, showing the aluminum hydroxide particles adhering to the filter	29
Figure 11. SEM BSE image and EDS X-ray spectrum of the dry swipe from the residue location	30
Figure 12. SEM SE image and element maps of the dry swipe from the residue location	31
Figure 13. SEM SE images of insect fragment on the dry swipe sample from the residue location	32
Figure 14. SEM BSE images of the particles from the wet swipe of the residue location	34
Figure 15. SEM SE image, element map, and X-ray spectrum of the particles from the wet swipe of the residue location	35
Figure 16. SEM BSE images of the insect fragment on the wet swipe of the residue location	36
Figure 17. Boroscope camera images of insects on the floor of the HBU storage cask. The scale is not provided in the images, but comparison with structural features in the images (not shown), indicates that the insects are 2-4 mm in size. Note that each image is independent, the smaller images do <i>not</i> represent higher magnification views of the insects in the single larger image.	37

TABLES

Table 1.	Corrosion Residue Samples from the High-burnup Demonstration Cask	.17
Table 2.	Elemental Composition of the HBD Cask Corrosion Samples, in µg/sample	.40
Table 3.	Elemental Composition of the HBD Cask Corrosion Samples, in µg/sample (blanks	
subtr	racted)	.40
Table 4.	Elemental compositions, normalized to the Aluminum Content in Each Sample	.40

NOMENCLATURE

BSE backscattered electron [imaging]

DOE Department of Energy

EDS energy dispersive [X-ray] spectroscopy

EPRI Electric Power Research Institute FME foreign material exclusion [cover]

FTIR Fourier Transform Infrared [Spectroscopy]

HBU high-burnup [demonstration project]

ICP-MS inductively coupled plasma-mass spectrometry ISFSI independent spent fuel storage installation

SCC stress corrosion cracking
SE secondary electron [imaging]
SEM scanning electron microscope

SNF spent nuclear fuel

SNL Sandia National Laboratories

XRD X-ray diffraction

1. INTRODUCTION

This report documents the results of analyses of corrosion residues found within the cask that will be used for the high-burnup demonstration (HBU) project when it was opened for inspection after several years in storage. The TN-32B cask was fabricated by Precision Custom Components of York, Pennsylvania in April, 2004 and was stored there until May, 2015, when it was shipped to Columbiana Hi Tech LLC in Greensboro, North Carolina to be modified for the HBU test. On September 29-30, 2015, a team consisting of Electric Power Research Institute (EPRI) personnel, AREVA personnel (AREVA Federal Services, AREVA TN, and AREVA P&T), and personnel from Dominion Engineering Virginia Power performed an inspection of the cask. As part of the inspection, the cask was opened and the interior components surveyed. During this survey, polyethylene-wrapped wooden cribbing that had been placed within the cask over 11 years earlier to prevent shifting of the basket during transport was removed, revealing two small areas of brownand-white residue on the aluminum basket rails. These areas are shown in Figures 1 and 2. The residue appeared to be a corrosion residue, and although it was likely that this was somehow caused by contact with the wooden cribbing, there was some concern that it could have been caused by some contaminant on the metal itself, and that it could occur elsewhere within the cask, where it would not be as readily observed. To test this, the decision was made to collect samples of the suspected corrosion residue the next time the cask was opened. In July, 2016 the cask was opened for a fit-up test, and the samples were collected. The samples were sent to Sandia National Laboratories (SNL) for analysis. Also during this test, a boroscope was lowered though the basket to the bottom of the canister, to look for further evidence of corrosion.

The material sent to SNL consisted of a single bulk sample of the filamentous spongy residue, and several samples collected by swiping the residues at each of the two locations with 5-inch paper filters. At SNL, the samples were removed from their sample tubes and photographed. Then, subsamples were taken for imaging and textural analysis by scanning electron microscopy (SEM) and compositional analysis using an energy dispersive X-ray system (EDS) attached to the SEM. Sub-samples were also analyzed by X-ray diffraction (XRD). Finally, the bulk of each sample was calcined (ashed), digested, and analyzed using inductively-coupled-plasma mass spectrometry (ICP-MS) to determine the elemental composition of the residue. This report documents the results of those analyses. The samples received by SNL and the analytical techniques used to analyze them are described in Section 2; Section 3 presents the results of the different analyses; and the results are discussed and interpreted in Section 4. Conclusions are provided in Section 5.

As discussed in the following sections, the residues consist largely of aluminum corrosion products, fungal material, and organic compounds. Insect fragments were also present in the samples collected. Trace element analyses indicate that the elements present in the residues are sourced to both the aluminum alloy and to degradation of the wood. Given evidence for fungal growth after the cask was sealed, it is concluded that the wooden cribbing was infested with fungi and possibly, with living insects as well, when it was placed in the cask. Several possible causes for the observed attack are considered, including crevice corrosion, oxic corrosion due to corrosive wood treatments potentially present in the cribbing, and corrosion due to organic compounds leached from the wood and produced by fungal action. Regardless of the mechanism, it is clear that corrosion of the aluminum metal was due to contact with the wooden cribbing. Once the cask

has been thoroughly cleaned, further corrosion over the course of the high-burnup demonstration test is unlikely.

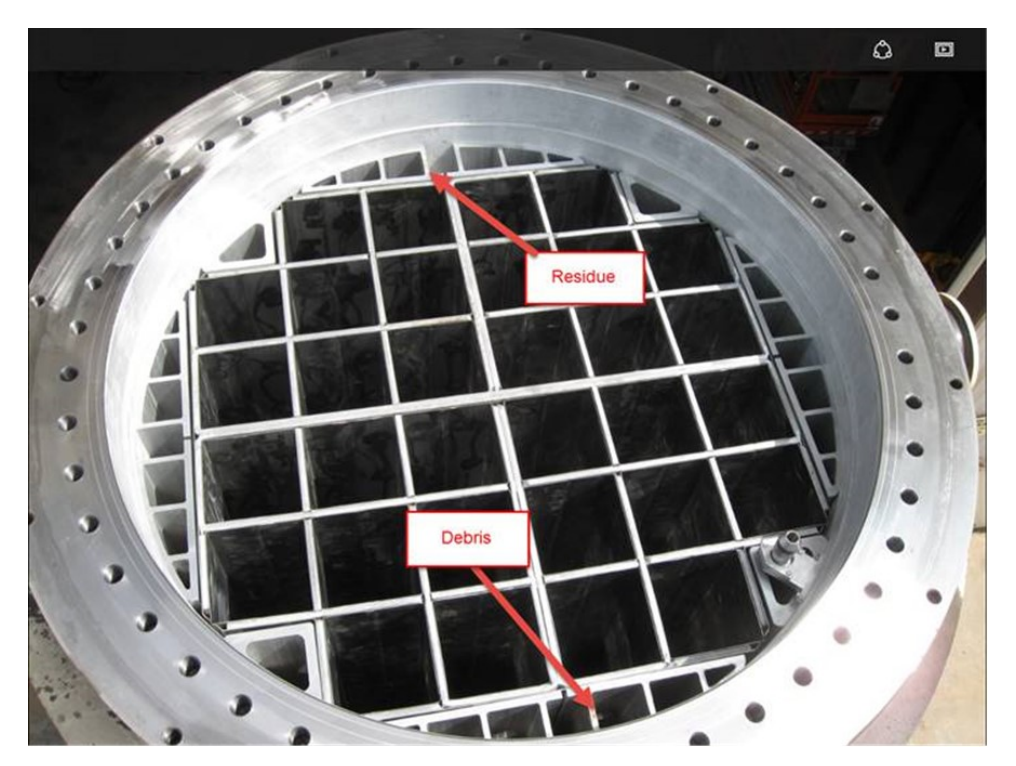


Figure 1. Photograph of the storage cask, with the lid removed. The locations of the two areas with apparent corrosion residue are shown.

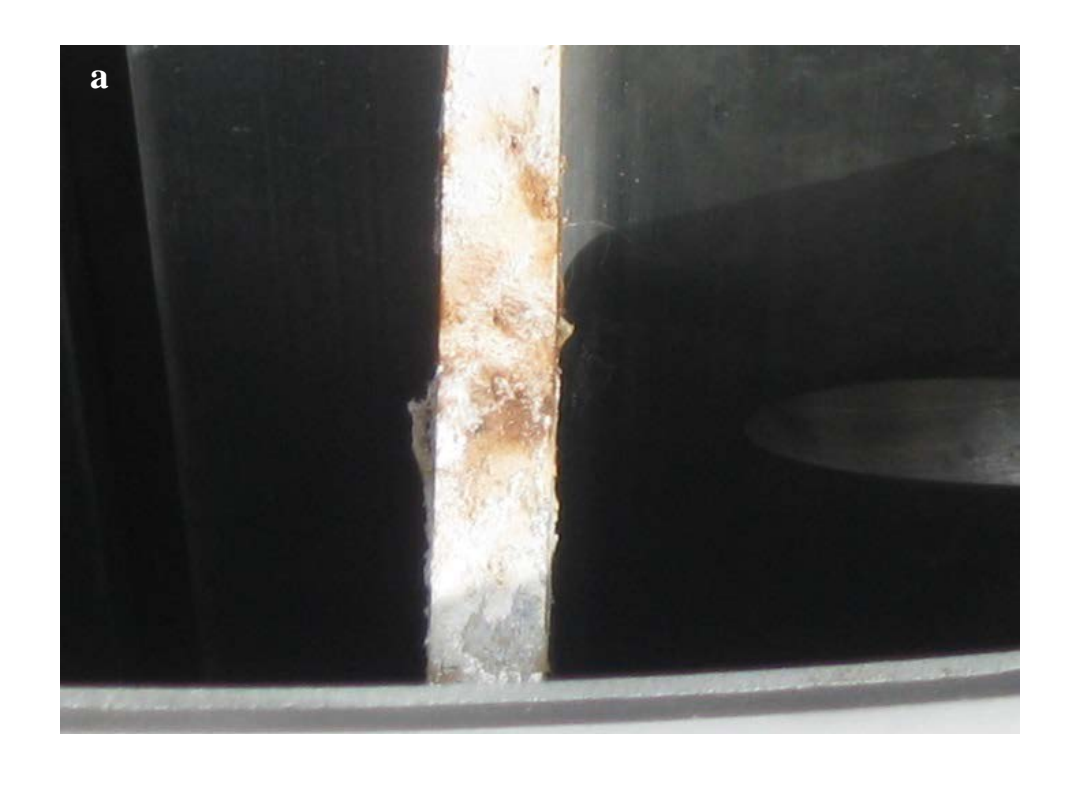




Figure 2. Photographs of a) the "debris" on the basket rail (near side), and b) the "residue" on the basket rail (far side).

2. SAMPLES AND METHODS

2.1. Samples

Samples were collected from two locations on the aluminum basket rails, the "Debris" side, and the "Residue" side. The Debris side had finely fibrous mat of material that was partially detached from the surface (Figure 2a). The Residue side had a thin coating of material that was more strongly attached to the rail (Figure 2b). During sample collection, tweezers were used to collect a fragment of the loose debris from the Debris side. The material consisted of the fibrous base, with sand-sized grains attached and embedded in the fibrous material. The mat was stained brown in some areas, and the grains, although mostly white, were also stained in some areas. The debris sample was slightly over 1 cm in diameter. Following collection of the debris, swipes were taken of both sides, first a dry swipe, and then two wet swipes. The round 5" filters were folded and placed in 50 ml polypropylene sample vials for shipment to Sandia. Upon delivery to Sandia, the samples were photographed, and then a small piece of each was taken for SEM analysis. For chemical analysis, the two wet swipes from each location were combined, as there was no reason to analyze them individually. The samples are listed in Table 1 below. Images of the samples are shown in Figure 3 (note that only one of each pair of wet swipes is shown). The residue itself appeared to be a finely fibrous brown material, with white particles scattered across the top, and adhering to the fibers. The residue on the dry filters appeared to be a brown stain, finely granular. The residue on the damp filters was also a brown stain, but was more coarsely granular, with brown or white sand-sized grains.

Table 1. Corrosion Residue Samples from the High-burnup Demonstration Cask

Sample Description	Sample Type
Debris side – Debris	Loose debris
Debris side – Dry (dry swipe)	Filter paper
Debris side – Wet (wet swipe)	Filter paper
Debris side – Wet (2 nd wet swipe)	Filter paper (two filters)
Residue side – Dry (dry swipe)	Filter paper
Residue side – Wet (wet swipe)	Filter paper
Residue side – Wet (2 nd wet swipe)	Filter paper
Filter paper blank	Filter paper
Demineralized water blank (used to wet filters)	Aqueous solution

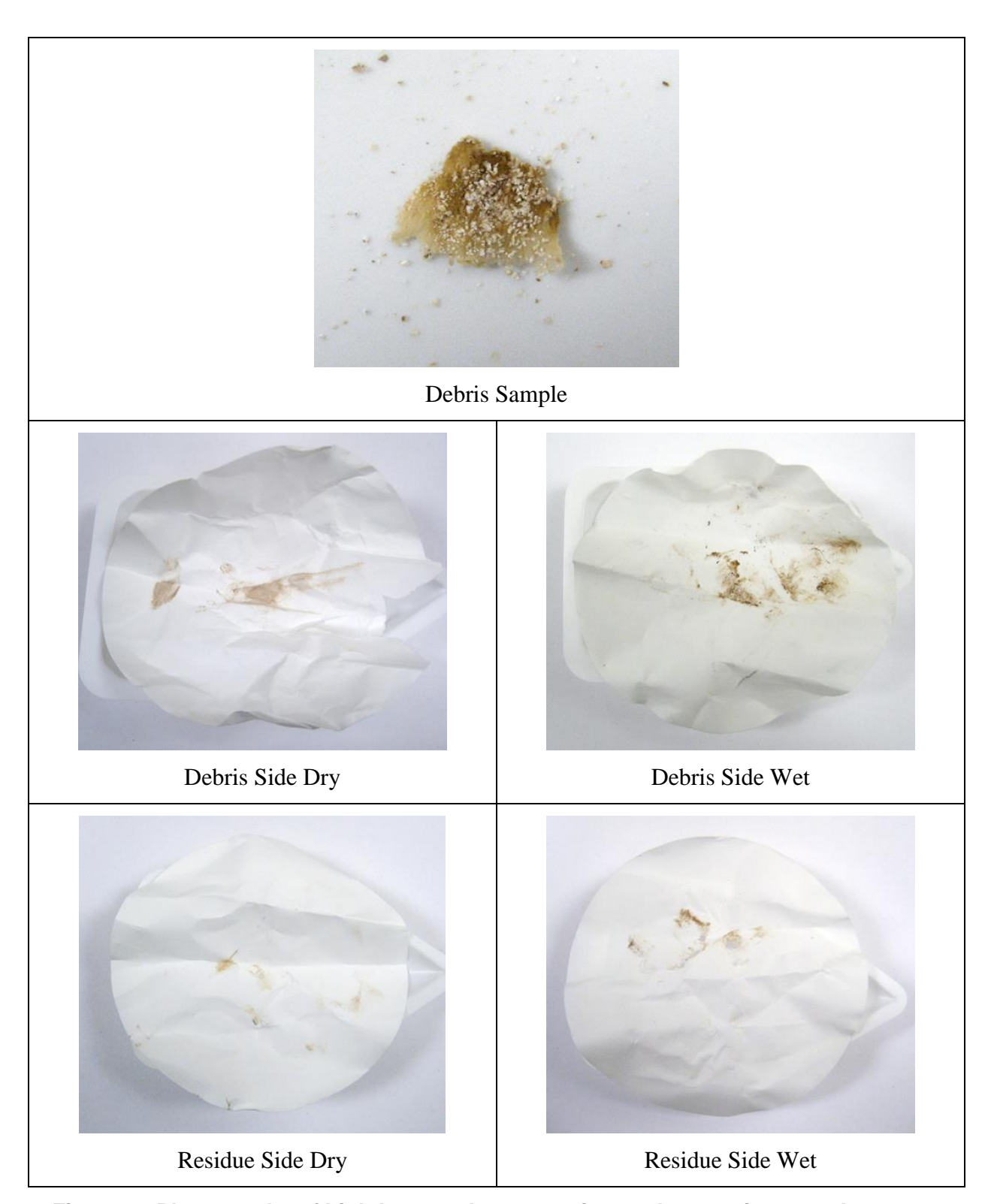


Figure 3. Photographs of high-burnup demonstration cask corrosion samples.

2.2. Methods

The following methods and equipment were used to characterize the samples from the high-burnup demonstration cask:

- *SEM imaging and EDS element mapping*. SEM/EDS analysis of the samples provides textural and mineralogical information of the corrosion residue, and allows visual identification of organic matter (floral/faunal fragments).
- X-ray diffraction analysis. XRD analysis identifies inorganic phases present, if crystalline.
- Fourier Transform Infrared Spectroscopy (FTIR)/Raman analysis. These complementary techniques provide information on the molecular bond structure of the materials analyzed, aiding in the identification of specific compounds.
- Chemical analyses of the filter samples and corrosion residue. Both the corrosion residue sample and the filter samples were calcined (ashed), digested, and analyzed by ICP-MS to determine bulk elemental composition of the residue.

SEM Imaging and EDS Analysis

SEM/EDS analysis of the samples provides textural and mineralogical information of corrosion residue components, and allows visual identification of organic matter (floral/faunal fragments). Sample fractions retained for SEM analysis were coated with carbon to reduce sample charging during analysis. Imaging and element mapping was done with a Tescan Vega3 SEM, equipped with an EDAX Element[©] EDS detector. An accelerating voltage of 20 keV was used, and working distances of 9 to 12 mm, with varying degrees of magnification. Images were obtained using both secondary and backscattered electron imaging, with a beam current of 100-200 pA. A somewhat higher beam current (1 nA) was used to produce a high count rate during EDS analysis and to facilitate rapid element mapping. However, the elevated beam current did enhance sample charging for the fibrous pad samples, resulting lower image quality in some cases.

XRD Analysis

XRD analysis was performed using a Bruker D2 Phaser diffractometer with a Cu K α X-ray source, and a LynxEye solid-state energy discriminating X-ray detector. Analyzed samples consisted of grains extracted from one of the wet pads from the "residue" location, and loose grains associated with the "debris" sample. The grains were crushed in a mortar and pestle and then slurried onto a zero-background silicon wafer prior to analysis. However, when analyzed, no peaks were observed. On the basis of textural and compositional data determined by SEM, the granular material is inferred to be amorphous aluminum hydroxide.

FTIR/Raman analysis

FTIR analysis was carried out using a Nicolet Nexus 870 FTIR instrument, with an optional Attenuated Total Reflectance "Durasamplir" accessory. Components in the infrared spectra were identified by functional group analysis combined with comparison to a reference library of infrared spectra. Raman spectroscopy was carried out using a microscope-based Raman spectroscopy with a laser light source. Incorporating a microscope into the Raman system makes possible resolution and detection on the microscopic scale. For this analysis, individual grains of the corrosion product from both the "residue"

location and the "debris" location were analyzed. The mineralogy of the grain was evaluated by comparison of the collected spectra to a reference library of Raman spectra.

Chemical Analysis

Following removal of small fragments for analysis by SEM/EDS and XRD, the remainder of each sample was placed in a 15 ml platinum crucible and ashed. The wet filter samples from each sample location were combined for analysis. The residue was then digested using 4 ml Optima®-grade hydrofluoric acid and 2 ml Optima®-grade nitric acid. The sample was taken to dryness on a hot plate and then redissolved in Optima®-grade hydrochloric acid. The hydrochloric acid converts insoluble fluorides into readily dissolved chlorides, and also dissolves iron oxides that do not readily dissolve in nitric acid. After taking the hydrochloric acid back to dryness, the residue was redissolved in concentrated nitric acid, taken to dryness again, and then taken up in 15 ml 2% nitric acid for analysis by ICP-MS.

The samples were analyzed using a Perkin-Elmer NexION 350D inductively-coupled plasma mass spectrometer (ICP-MS), using the Standard, Collision, and Reaction modes for individual isotopes. Prior to quantitative analysis, the samples were surveyed using a semi-quantitative procedure to determine what elements were present and approximate concentrations. This information was used to develop a set of calibration standards for quantitative analysis from high-quality Perkin-Elmer ICP-MS stock solutions. All stock solutions had expiration dates from March to April, 2017. A blank and five calibration standards were used for the quantitative analysis. Standard concentrations were 3, 10, 30, 100, and 1000 ng/ml. Samples were diluted until they fell within the range of the standards. The ICP-MS has extremely high sensitivity, with good signals for even the lowest standard (3 ng/ml).

3. RESULTS

3.1. SEM/EDS Analysis

SEM/EDS analysis of the samples was carried out to determine corrosion residue texture, bulk composition, and mineralogy. The samples are listed in Table 1, and those that were analyzed include a fragment of the debris; a piece of the dry filter pad with adhering brown material from the "debris" location; a piece of the dry pad from the "residue" location with adhering brown material; and loose grains extracted from the surface of the wet pad from the residue location. SEM images were taken of characteristic features and EDS element mapping was done to assess mineralogy and composition. Results are summarized here with typical images from the samples.

SEM images were taken both in backscattered electron (BSE) mode and in secondary electron (SE) mode. In BSE images, the relative brightness of the different phases present indicates the average atomic number (Z); materials with a higher average Z scatter more electrons, and appear brighter that materials with a lower average Z. SE images emphasize texture over composition, and because they must be taken at high vacuum, charging is a greater problem. The SE images presented here were taken mostly because that is the only option available when doing EDS mapping and analysis on the SEM used.

3.1.1. Debris

A small fragment of the debris was removed from the larger piece, and carbon-coated for analysis by SEM/EDS. Figures 4 through 7 are backscattered electron (BSE) SEM images of the debris. The material consists of a fibrous tangled mat of material, with coarse angular grains over the surface and embedded within the mat. The granular material adheres to the mat, encapsulating the fibers in some places, and in several areas appears to have formed by disaggregation of a larger, more continuous deposit (Figure 5). Point X-ray analyses in Figure 5 show that the fibrous material is organic, consisting mostly of carbon (C) and oxygen (O) with small amounts of potassium (K) and phosphorous (P); very small iron (Fe) peaks were also observed. X-ray spectra for the granular material showed only aluminum (Al) and O, in some cases with a small peak for K.

Figure 6 shows the fibrous organic material at higher magnification. The material is a tangled mass of intergrown branching and anastamosing fibers. This material appears to be a fungal mycelium, consisting of branching filamentous hyphae. Figure 7 illustrates the texture of the granular material; it is generally covered with shrinkage cracks, and in areas, shows a botryoidal structure, indicating it formed as a gel. During mapping and point analysis (when the beam current was increased), heating by the electron beam caused decrepitation of the sample, indicating that it contained water. The material is interpreted to be hydrous amorphous aluminum hydroxide, consistent with the lack of diffraction peaks when analyzed by XRD (Section 3.2). Hydrogen is not detectible by X-ray analysis, and aluminum oxide would show an identical EDS X-ray spectrum; however, aluminum oxide does not generally form an amorphous phase (Lee et al., 2009). To verify the identity of the phase, particles were analyzed by Fourier Transform Infrared Spectroscopy (FTIR), and Raman Spectroscopy. FTIR spectra showed very broad peaks due to the amorphous nature of the material, and were dominated by peaks for water/OH and for Al-O bonds. No carbonyl or carbonate signal was detected, but a single peak was present that did not

match any inorganic aluminum phase and apparently represents organic material. Raman spectroscopy proved difficult due to sample fluorescence caused organic compounds in the samples. The Raman spectra that were collected were of poor quality, but had small, broad peaks that probably represent organic or aluminum-organic complexes, although no unique matching phase was identified in the Raman spectral database. In short, the material appears to be hydrous amorphous aluminum hydroxide, with an undetermined amount of organic material, possibly present as an aluminum organic complex. It is unlikely that the organic component is large, however. The samples were carbon coated for analysis, but despite this, most of the EDS analyses that were collected from the materials had only small carbon peaks (a few did have large peaks). The organic material may be organic acids leached from the wood as it decayed, a process probably enhanced by fungal action, or may be exometabolites produced by the fungi itself.

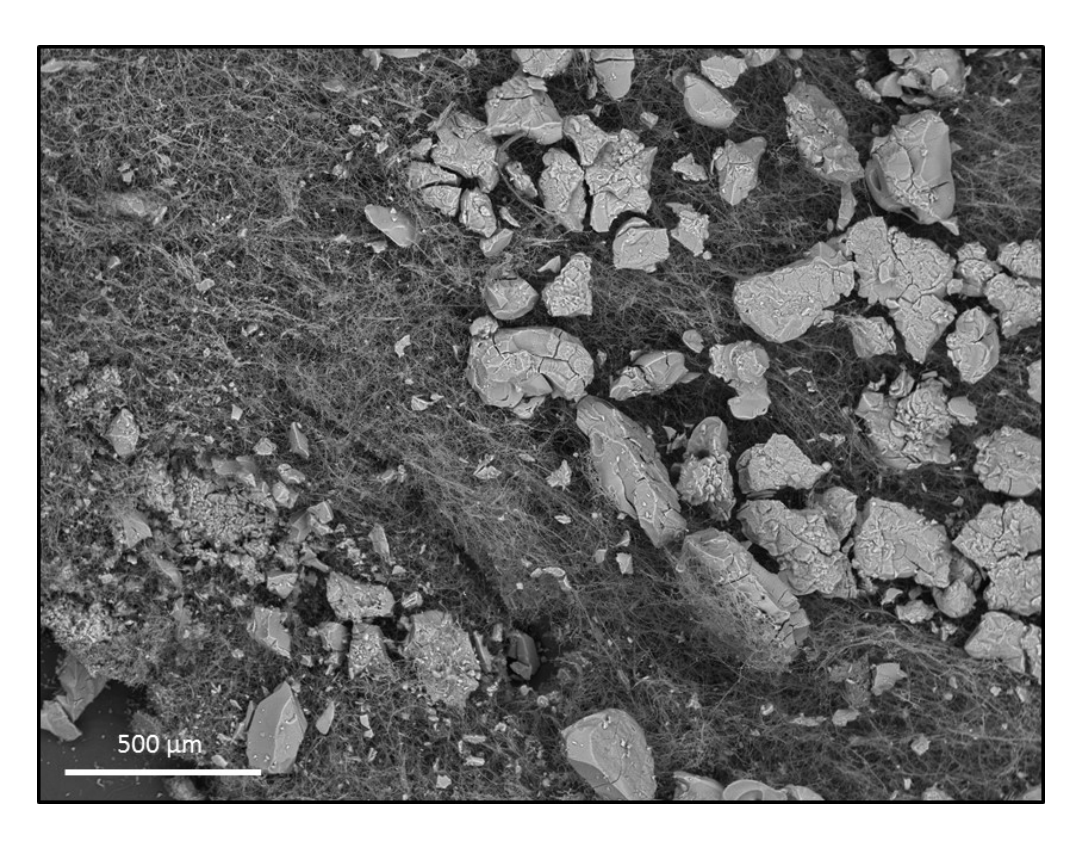


Figure 4. SEM BSE image of the Debris sample, showing the filamentous fungal matrix and the adhering amorphous aluminum hydroxide.

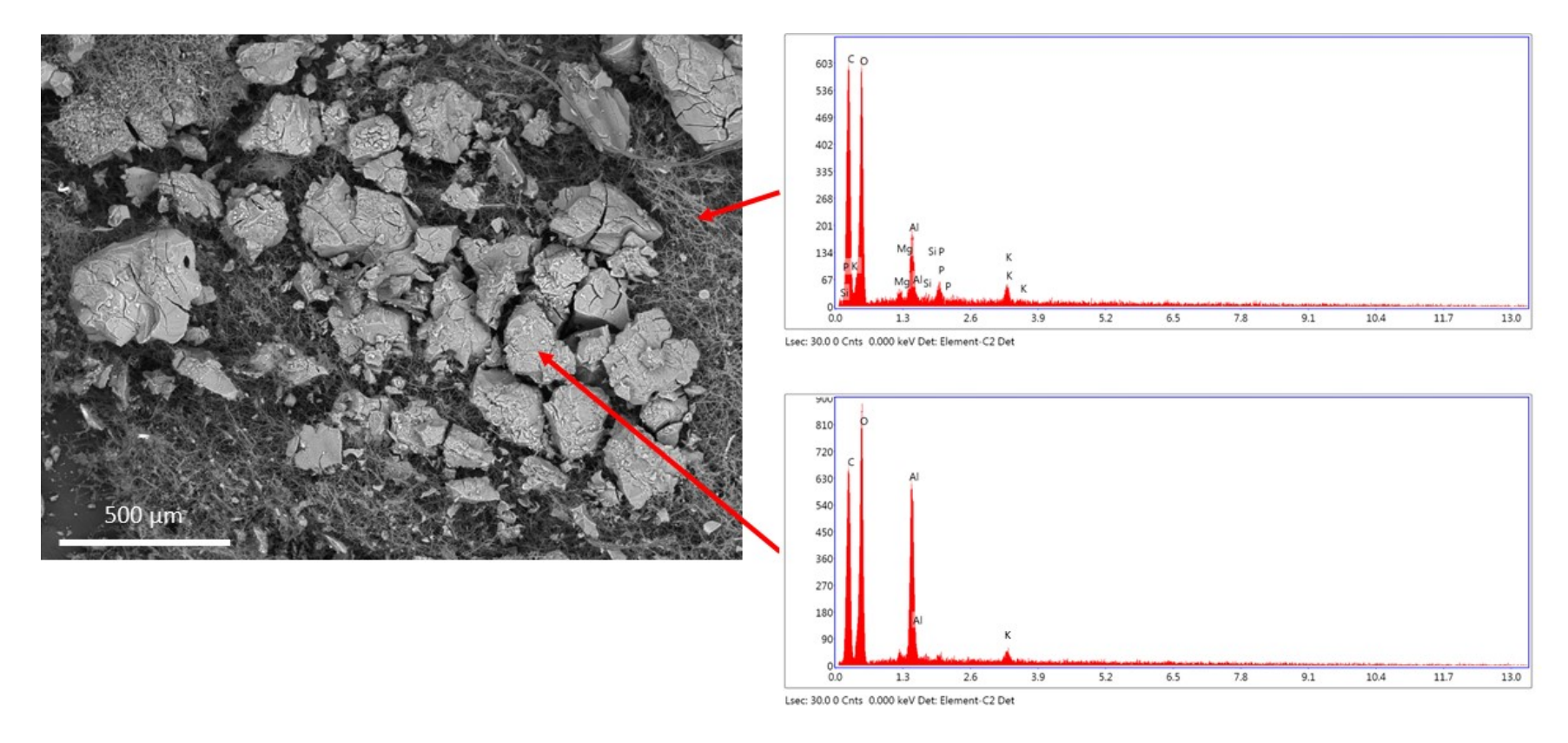


Figure 5. SEM BSE image of the Debris sample, showing the filamentous fungal matrix and the adhering amorphous aluminum hydroxide.

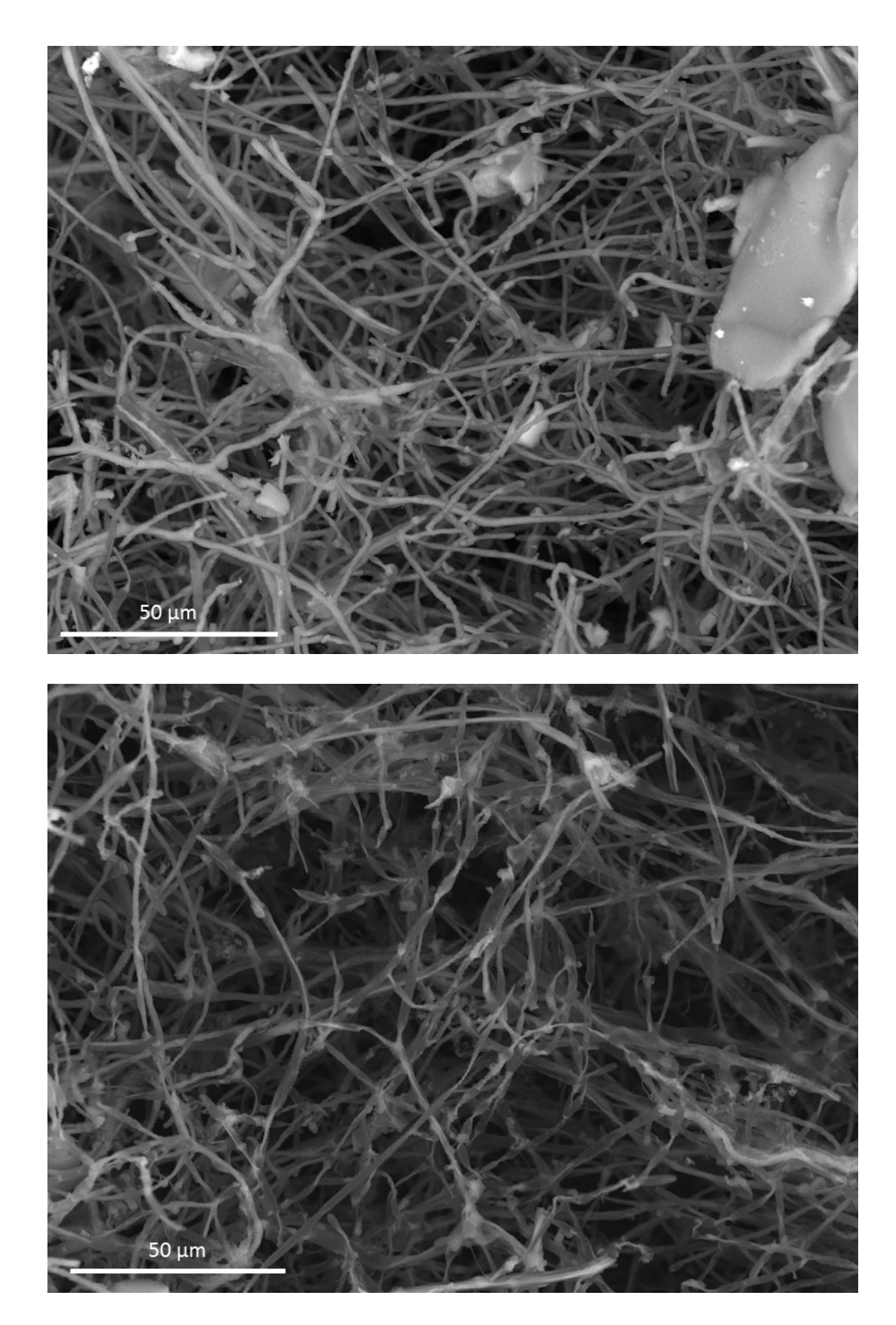


Figure 6. SEM BSE images of the Debris sample, showing close-up images of the fungal mat.

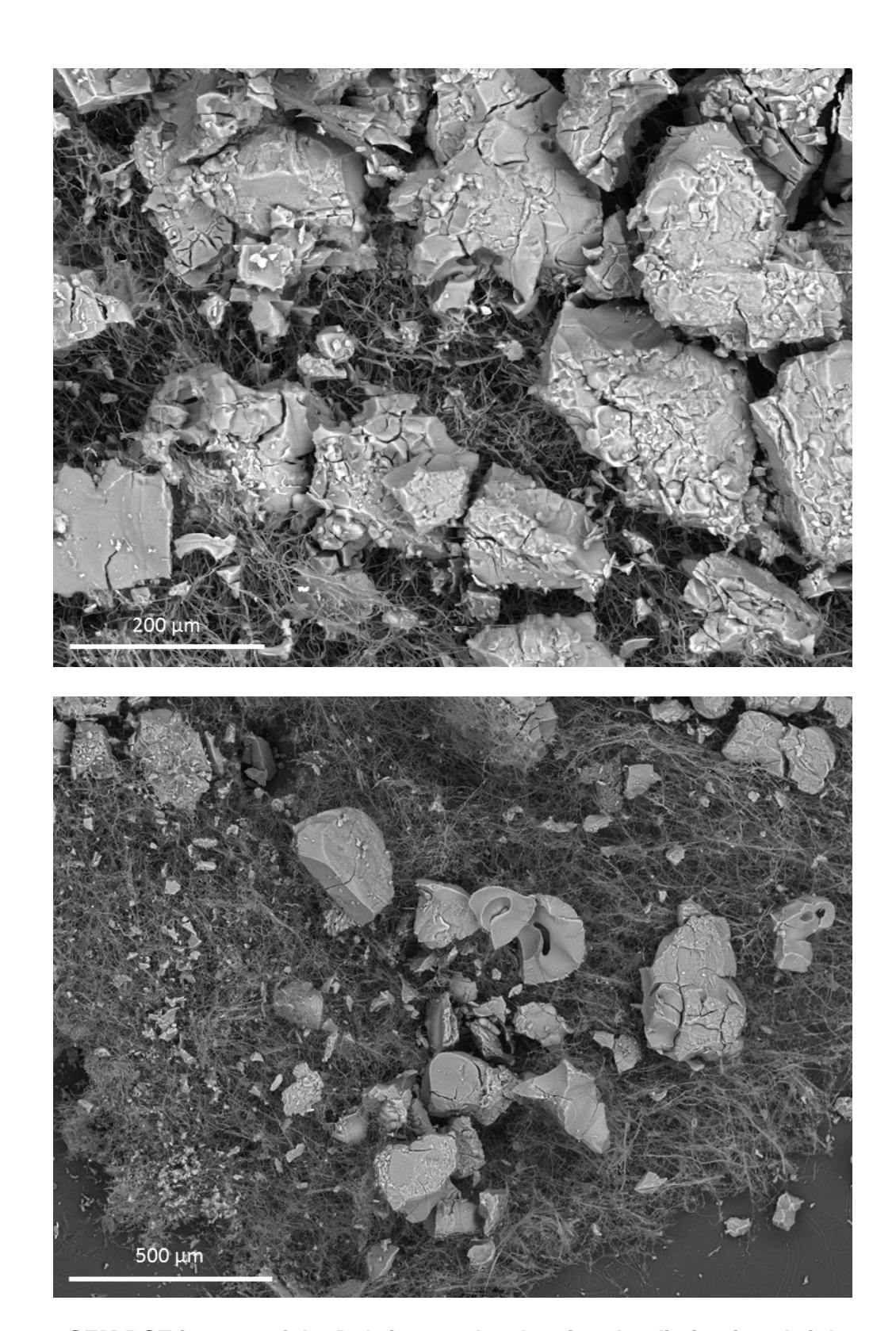


Figure 7. SEM BSE images of the Debris sample, showing the distinctive shrinkage cracks and in some areas, botryoidal morphology of the aluminum hydroxide.

3.1.2. Dry swipe from the debris location

The dry swipe from the debris side had a brown discoloration, consisting of fine, dry material, that could be readily dislodged from the filter. A fragment of the filter was cut from the stain and analyzed by SEM. Figure 8 shows BSE images of the sample, illustrating the fine particles adhering to the fibrous filter. Figure 9 shows a SE image, element maps, and X-ray spectrum for the material on the filter. Spectral analysis of areas of the filter coated with many particles indicates that the material consists largely of aluminum hydroxide, but high concentrations of potassium are also present. The stain on the filters was brown in color, and it was originally considered possible that iron nails in the cribbing might have corroded to produce iron oxides. However, no separate iron phase was observed with the SEM. This was true for all locations examined. It seems likely that the brown discoloration is due to organic compounds (e.g., humic acids) derived from the wooden cribbing, rather than to iron oxides.

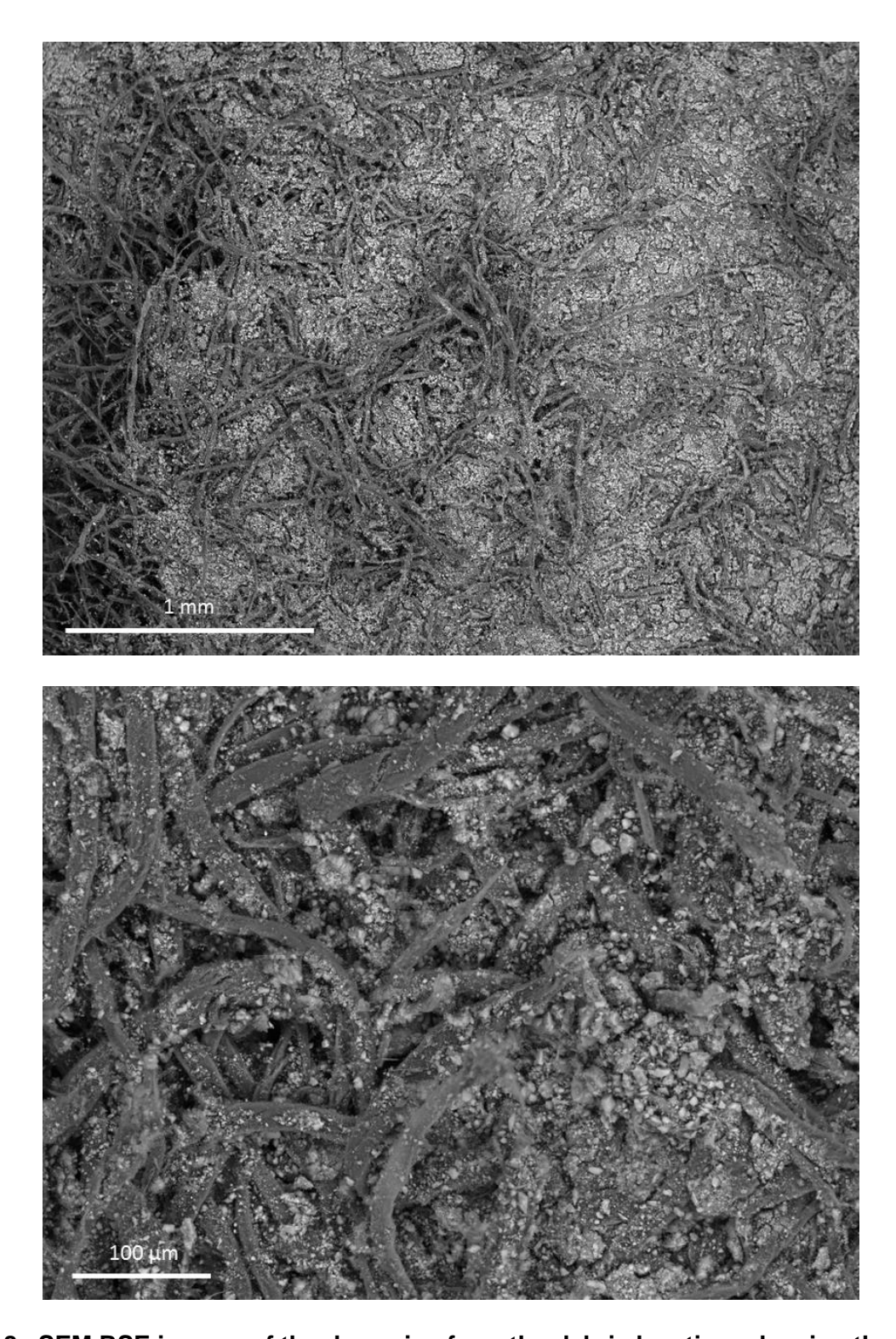


Figure 8. SEM BSE images of the dry swipe from the debris location, showing the aluminum hydroxide particles adhering to the filter.

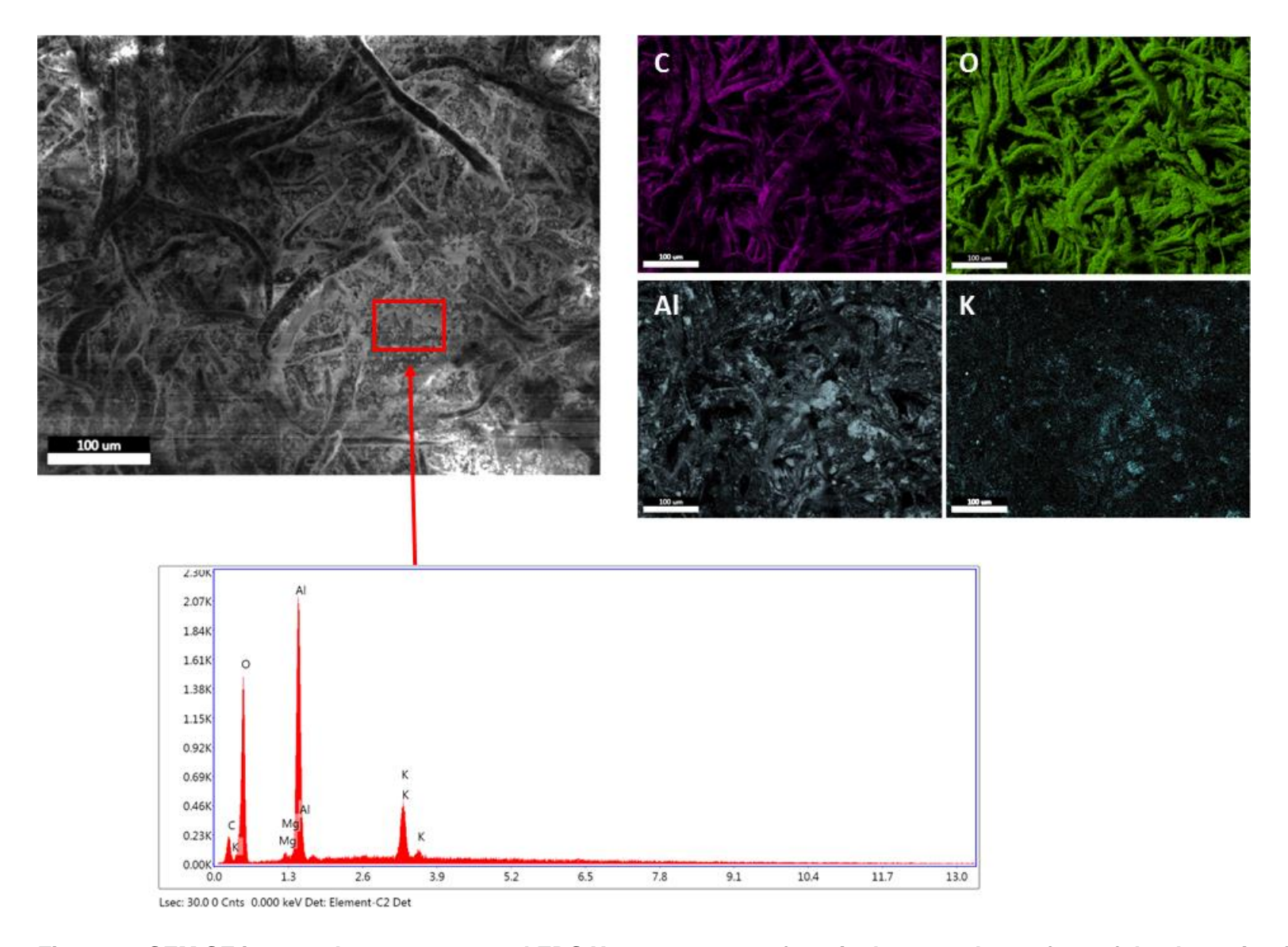


Figure 9. SEM SE image, element mays, and EDS X-ray spectrum of particulates on the surface of the dry swipe from the debris location.

3.1.3. Dry swipe from the residue location

SEM images of the dry swipe from the residue location are shown in Figures 10 and 11. As with the other dry swipe, this sample had a brown stain consisting of loose particles. The particles consist mostly of aluminum hydroxide, but a small amount of potassium is also present. X-ray element maps are shown in Figure 12, and indicate that small amounts of phosphate and magnesium are also present, at least in part as discrete grains. Once again, no discrete iron phase is present, once again suggesting that the brown coloration is due to organic compounds formed by fungal degradation of the wood. Relatively high concentrations of iron were observed in the chemical analyses of these samples (Section 3.3); the absence of an iron phase indicates that it was bound into the organic phase.

Also present on the dry swipe from the residue location is fragment of insect matter (Figure 13). The fragment consists of a small piece of material, covered with hairs and in some locations, scales. It is insufficient to identify the organism that it represents.

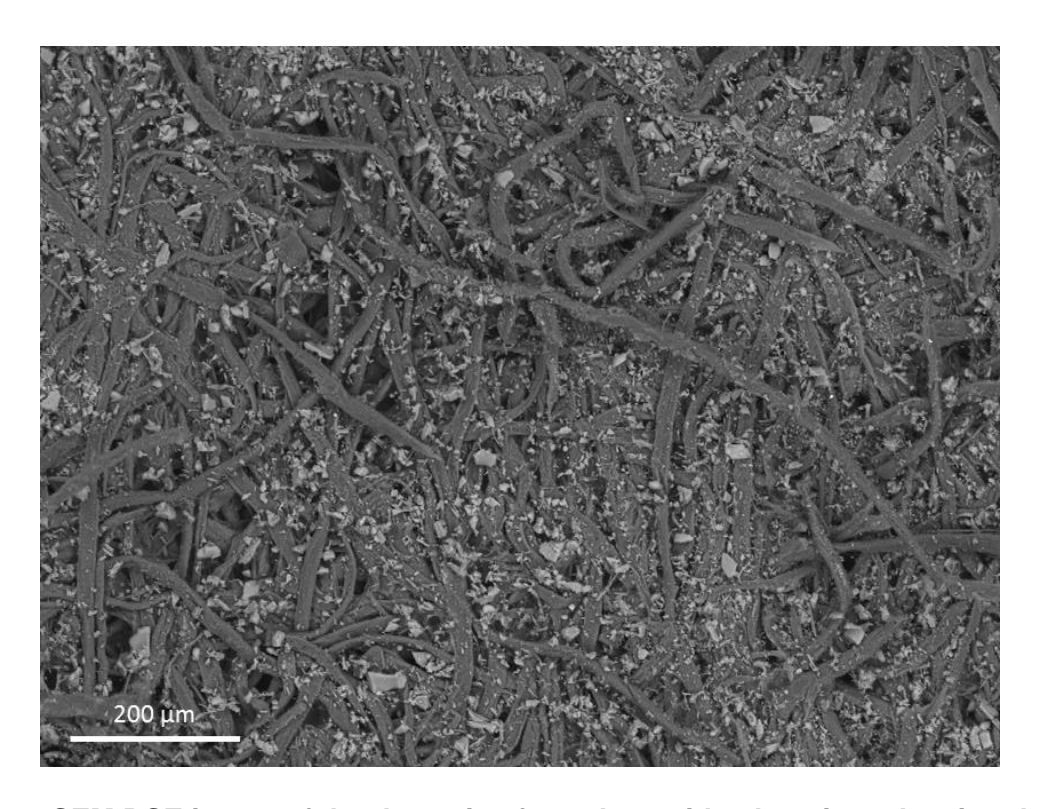


Figure 10. SEM BSE image of the dry swipe from the residue location, showing the aluminum hydroxide particles adhering to the filter.

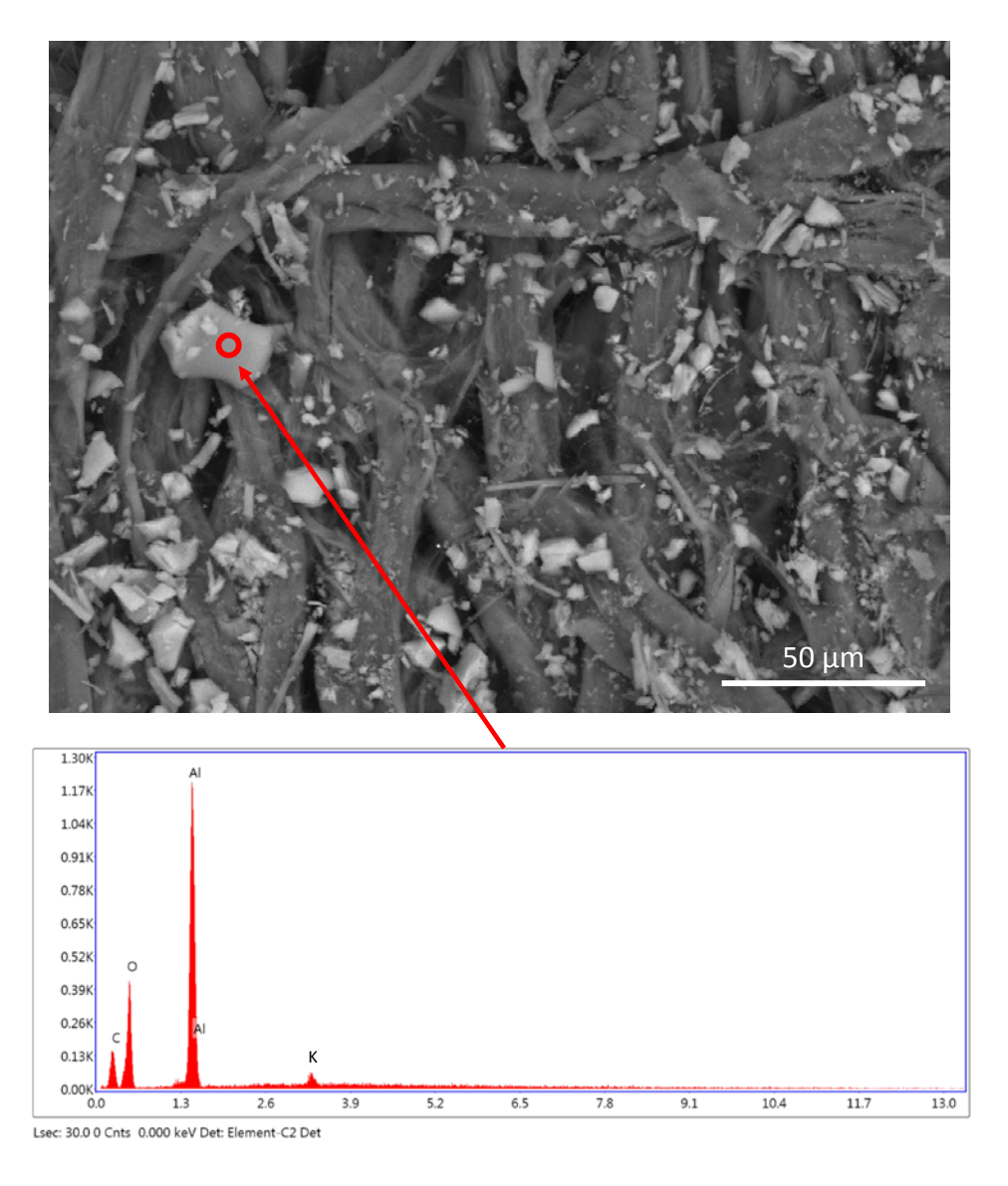


Figure 11. SEM BSE image and EDS X-ray spectrum of the dry swipe from the residue location.

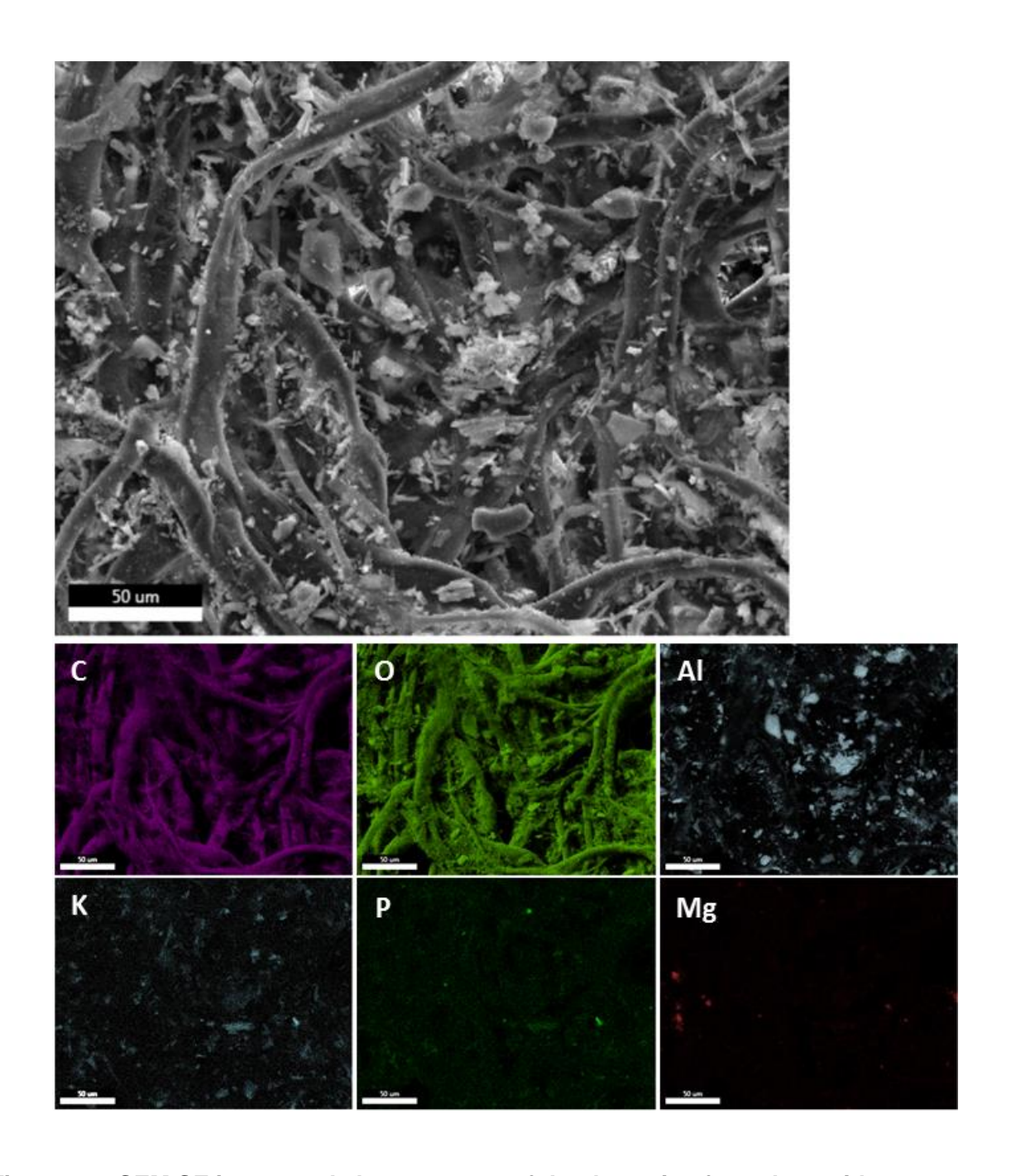


Figure 12. SEM SE image and element maps of the dry swipe from the residue location.

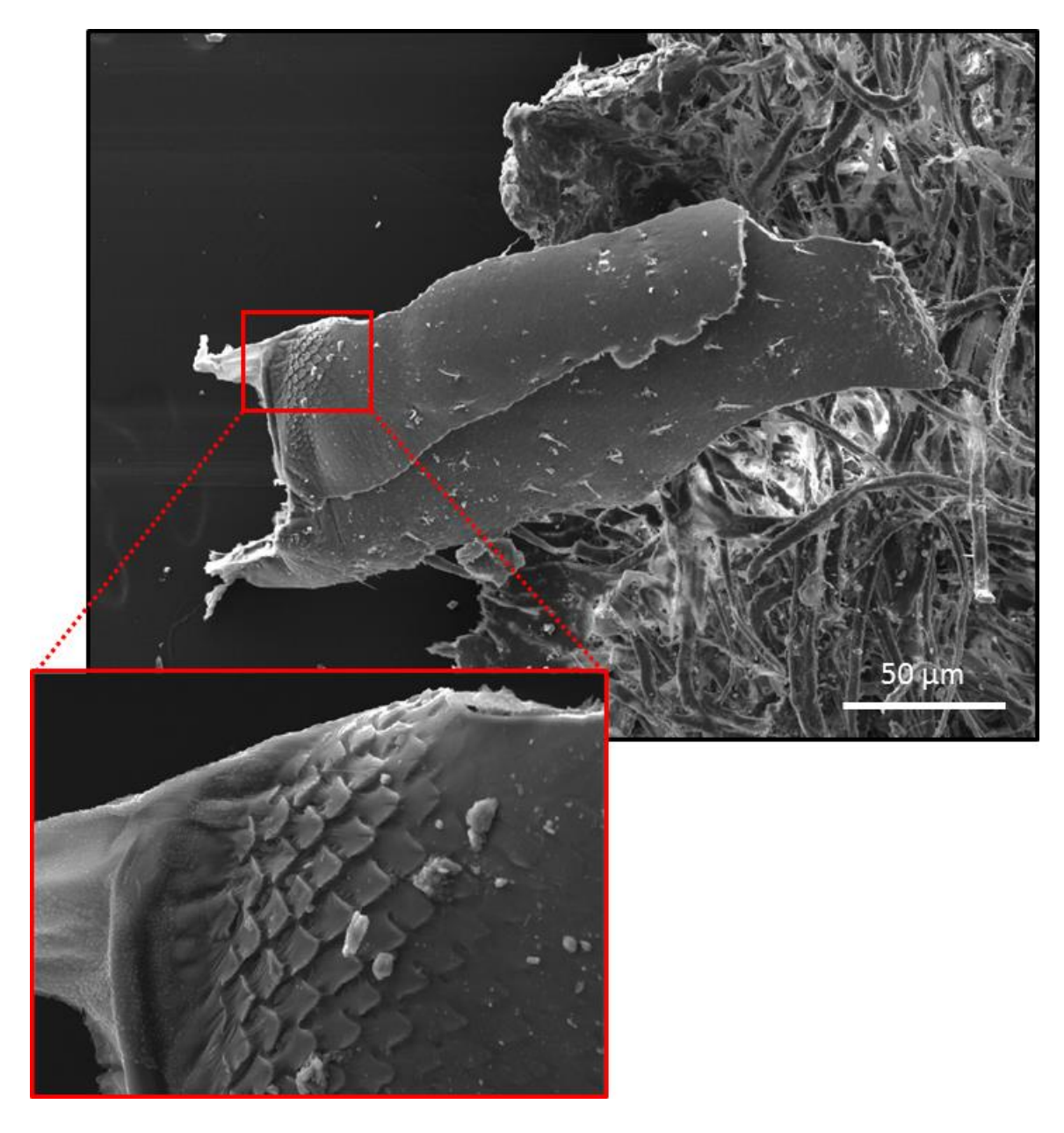
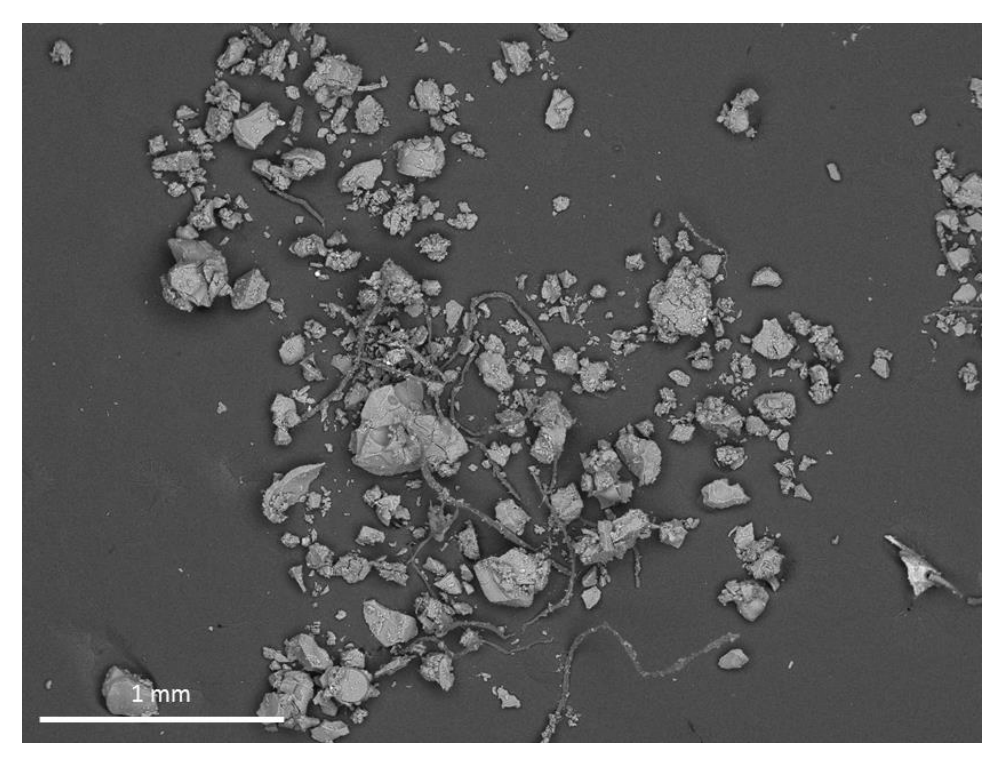


Figure 13. SEM SE images of insect fragment on the dry swipe sample from the residue location.

3.1.4. Wet swipe from the residue location

Two wet swipes were taken from the residue location. Both had brown staining; however, the first swipe also had coarse, sand-sized white particles adhering to it. Some of these were brushed off of the filter and mounted on carbon tape for SEM analysis. The particles are shown in Figure 14, and element maps are provided in Figure 15. The particles are aluminum hydroxide, with no detectible impurities, and have a similar morphology (shrinkage cracks) to the grains of aluminum hydroxide on the debris sample (Section 3.1.1). Note that in these clean, large grains of the amorphous material, it is clear that any organic component is very small, as the carbon peak is insignificant. An insect fragment was also present on this sample (Figure 16). The fragment appears to be part of an insect head; however, it is too incomplete to identify the type of insect.



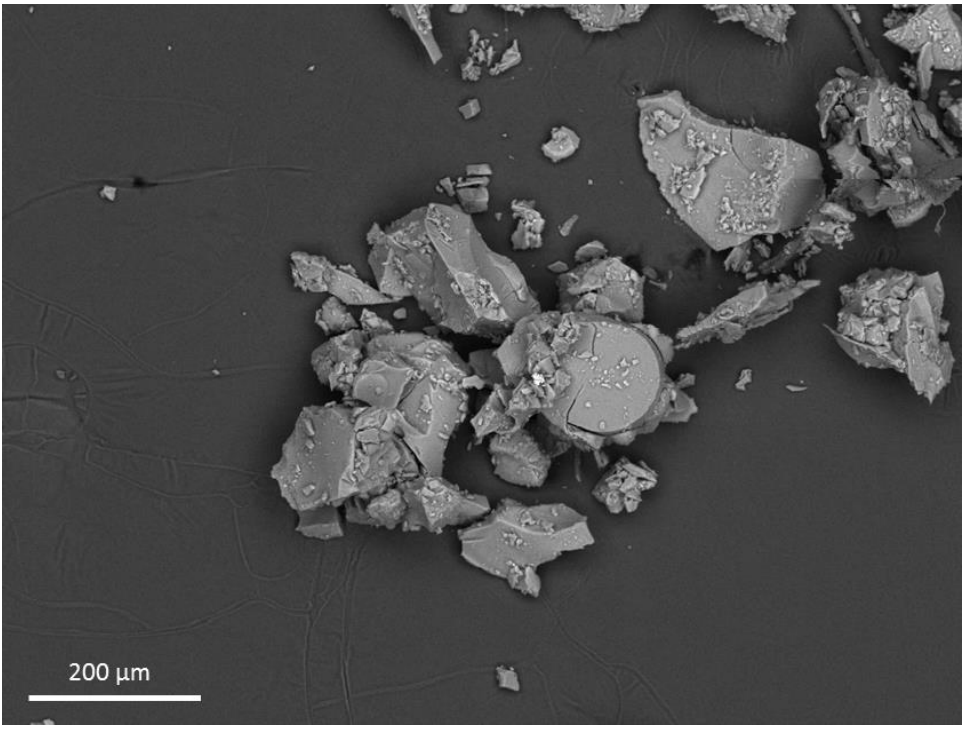


Figure 14. SEM BSE images of the particles from the wet swipe of the residue location.

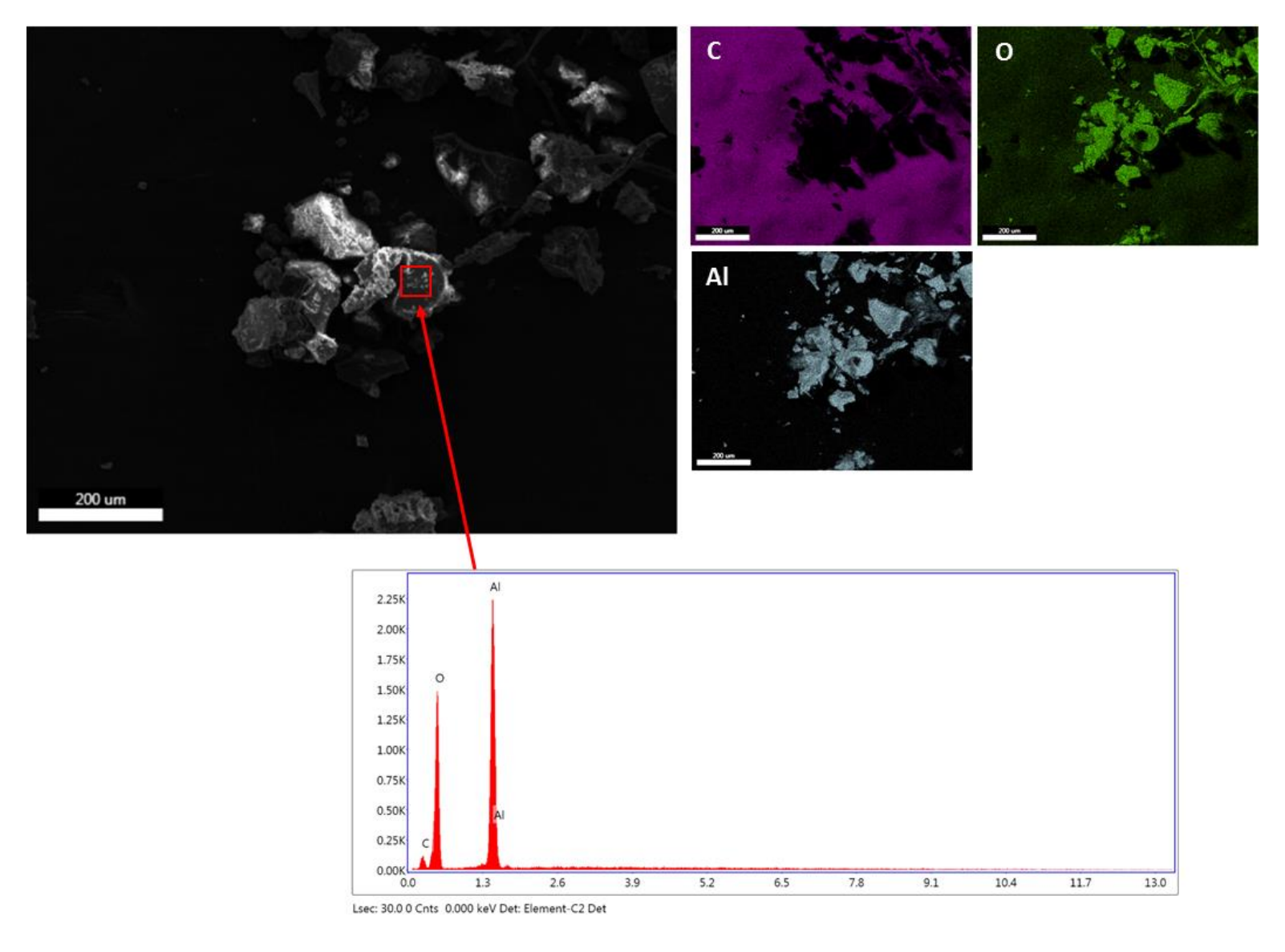


Figure 15. SEM SE image, element map, and X-ray spectrum of the particles from the wet swipe of the residue location.

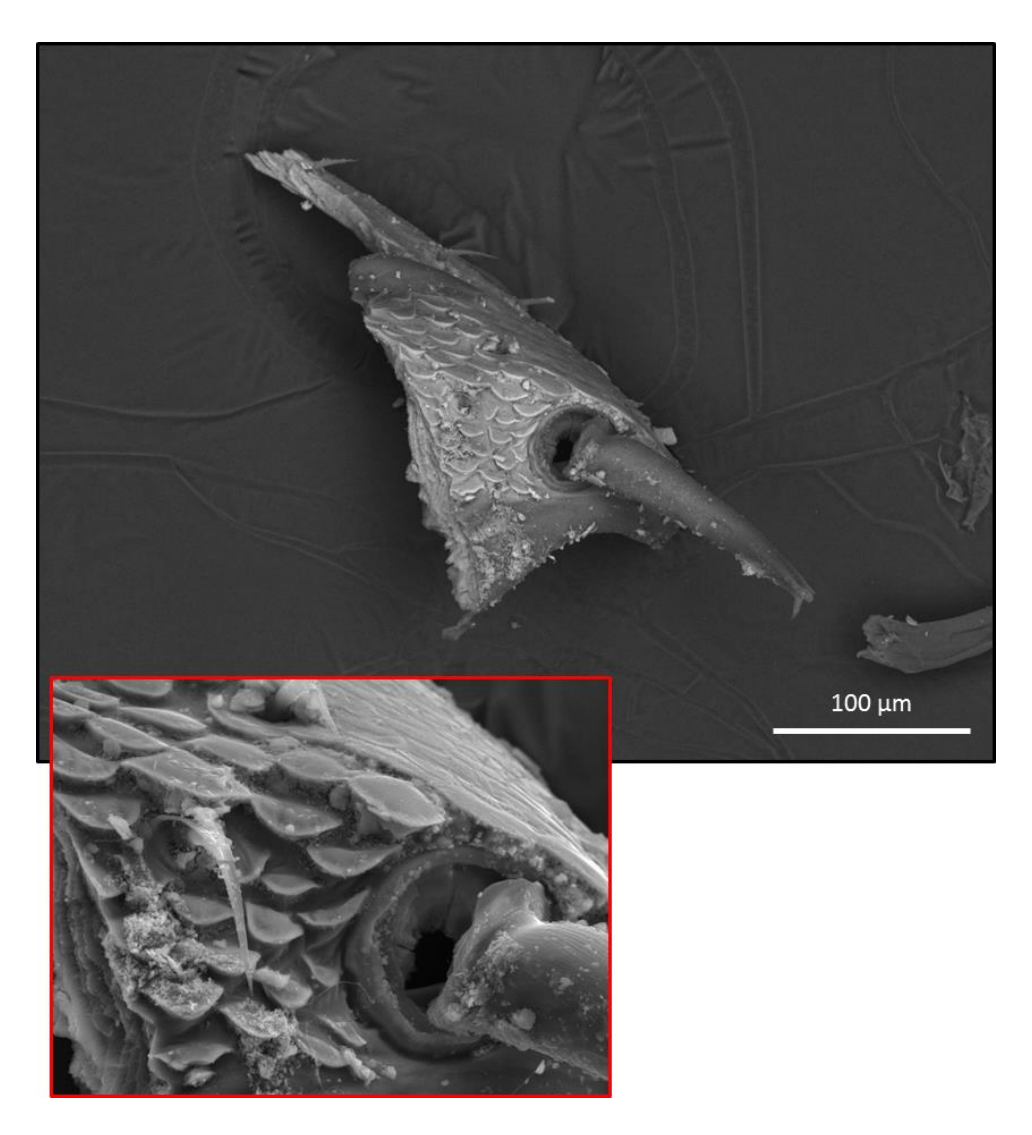


Figure 16. SEM BSE images of the insect fragment on the wet swipe of the residue location.

3.1.5. Discussion of the SEM data.

SEM analyses of the debris and the swipe samples indicate that most of the residue on the aluminum basket and rails consists of aluminum hydroxide, and indeed represents corrosion of the aluminum. The aluminum hydroxide corrosion residue is present as an amorphous material, that may have formed as a gel. The locations where corrosion occurred appear to be associated with biological activity. Debris present on the aluminum has been identified as fungal matter, and insect fragments have also been identified. These may be related. Several insects exist in a symbiotic relationship with fungi, including bark and wood-boring (ambrosia) beetles, and some species of tower termites and ants (Vega and Blackwell, 2005). The insects help disperse the fungi by transporting it to new locations. The beetles disseminate the fungi in their tunnels and brood galleries, where it grows on the exposed wood surface. The beetles and/or their larvae feed on the fungi growing on the wood surface and on fungus-colonized, partially degraded wood (Licht and Biedermann, 2012). Although other explanations are possible, it seems likely that wood or bark beetles were present in the cribbing when it was placed in the cask, and they inoculated the wood with the observed fungus. During the boroscope inspection of the cask, many small dead insects were observed on the floor of the cask. Photographs are shown in Figure 17; the photographs are of insufficient quality to identify the insects, but the identity can be determined when the cask is cleaned, if the dead insects observed at the bottom of the cask can be recovered and identified.



Figure 17. Boroscope camera images of insects on the floor of the HBU storage cask. The scale is not provided in the images, but comparison with structural features in the images (not shown), indicates that the insects are 2-4 mm in size. Note that each image is independent, the smaller images do *not* represent higher magnification views of the insects in the single larger image.

It is clear from the SEM photos (Figures 4,5, and 7) that the fungi were present before or during the corrosion process, as the corrosion products are deposited on top of the fungal mat, and as small particles scattered throughout the mat. Moreover, it is clear from the morphology of the fungal mycelium (Figure 2a), that the fungus grew over the surface of the aluminum. Hence, fungus growth occurred after the cribbing was placed in the cask and the cask was sealed. Similarly, the dead insects in the bottom of the cask suggest that living beetles were present when the cask was sealed. If they are indeed wood beetles, as we hypothesize, it seems likely that the insects actually pupated in the wood and bored out during storage, dying in the sealed cask.

3.2. XRD Analysis

XRD analysis was performed using a Bruker D2 Phaser diffractometer with a Cu K α X-ray source, and a LynxEye solid-state energy discriminating X-ray detector. Analyzed samples consisted of grains extracted from one of the wet pads from the "residue" location, and loose grains associated with the "debris" sample. The grains were crushed in a mortar and pestle and then slurried onto a zero-background silicon wafer prior to analysis. However, when analyzed, no peaks were observed, indicating that the material is amorphous. On the basis of textural and compositional data determined by SEM, the granular material is inferred to have formed as an amorphous aluminum hydroxide gel.

3.3. Chemical Analysis

The methods used for digestion and chemical analysis of the samples are described in Section 2.2. After digestion, the corrosion samples were analyzed using a semi-quantitative ICP-MS survey method to determine what elements were present. This analysis identified a suite of elements that were then analyzed using quantitative methods. The results of the quantitative analyses, including the analysis of the blank filter provided with the samples, are provided in Table 2. In Table 3, the blank-subtracted concentrations are given; it is important to note that the number of filters varied from sample to sample, so different blank filter values were subtracted from each sample.

A blank and five calibration standards were used for the quantitative analysis. Standard concentrations were 3, 10, 30, 100, and 1000 ng/ml. Samples were diluted until they fell within the range of the standards. The ICP-MS has extremely high sensitivity, with good signals for even the lowest standard (3 ng/ml). Based on analysis of the standards as unknowns, all values in Tables 2 and 3 are accurate to $\pm 5\%$ or better.

Al is by far the most abundant element, followed by K and Fe, and then by P and Mg. Other metals that are present in significant amounts are Cu, Mn, Cr, Zn, and Ti. Trace quantities of Ba, Pb, Ag, and Zn are also present. Most of these metals are in the aluminum alloy comprising the basket rails, and their concentrations are consistent the source being corrosion of the aluminum. The aluminum is ASTM B-221 6061-T6, which has the following compositional specifications:

- Si, minimum 0.4%, maximum 0.8% by weight
- Fe, no minimum, maximum 0.7%
- Cu. minimum 0.15%, maximum 0.4%
- Mn, no minimum, maximum 0.15%
- Mg, minimum 0.8%, maximum 1.2%

- Cr, minimum 0.04%, maximum 0.35%
- Zn, no minimum, maximum 0.25%
- Ti, no minimum, maximum 0.15%
- Other elements no more than 0.05% each, 0.15% total
- Remainder aluminum 95.85–98.56%)

In Table 4, the concentrations of these elements are normalized to the measured aluminum concentrations in each sample. The normalized range in AA 6061-T6 is also provided. With the exception of Fe, the values for each element fall within or very close to, the possible range in the aluminum alloy. It is likely that these elements can be sourced to corrosion of the aluminum.

Fe, and also K and P, which are not present in AA 6061-T6 in significant amounts, cannot be sourced solely to the aluminum. These elements are in or on the fungal material itself (Figure 5), but also are present in the dark stain on the dry swipes (Figure 9), which consists of stained particles of aluminum hydroxide. Based on the SEM results, the aluminum hydroxide itself does not display X-ray peaks for these elements (Figure 15), or displays only very small peaks (Figure 11). It is inferred that these elements are concentrated within the fungal matter, but also within the organic material forming the dark stain. The brown coating is probably mostly organic in nature, and contains compounds such as organic acids that complex the metal species present, including the Fe, K, and P.

Table 2. Elemental Composition of the HBD Cask Corrosion Samples, in µg/sample

Sample ID	K	Mn	Cr	Mg	Zn	Fe	Cu	Ti	Р	AI	Ва	Pb	Ag	Zr	# filters
Filter blank	0.2	0.1	0.0	2.6	2.1	5.1	0.7	0.5	0.1	5.5	0.2	0.1	0.2	0.0	1
Debris side dry	97	1.7	2.4	9.0	5.8	44	7.7	3.9	12	1280	0.7	0.2	0.2	0.3	1
Debris side wet	334	4.6	5.9	30	13	149	17	8.6	54	5230	2.6	0.7	0.9	21	3
Debris	39	2.2	0.5	8.7	1.5	10	2.5	0.5	6.6	1100	0.1	1.4	0.4	0.1	0
Residue side dry	38	1.2	1.4	13	4.1	43	5.1	3.3	11	1060	0.4	0.2	0.1	0.2	1
Residue side wet	169	3.7	4.7	24	7.4	100	21	6.5	53	4170	1.1	0.4	0.2	0.4	2

Table 3. Elemental Composition of the HBD Cask Corrosion Samples, in µg/sample (blanks subtracted)

Sample ID	K	Mn	Cr	Mg	Zn	Fe	Cu	Ti	Р	AI	Ва	Pb	Ag	Zr
Debris side dry	97	1.6	2.4	6.4	3.7	40	7.0	3.4	12	1270	0.5	0.1	0.1	0.3
Debris side wet	334	4.2	5.8	22	7.1	134	15	7.1	54	5220	2.0	0.3	0.4	21
Debris	39	2.2	0.5	8.7	1.5	10	2.5	0.5	6.6	1100	0.1	1.4	0.4	0.1
Residue side dry	37	1.0	1.4	10	2.0	38	4.4	2.8	11	1060	0.2	0.1	0.0	0.2
Residue side wet	168	3.5	4.6	19	3.1	90	20	5.6	52	4160	0.8	0.1	0.0	0.4

Table 4. Elemental compositions, normalized to the Aluminum Content in Each Sample.

Sample ID	Fe	Cu	Mn	Mg	Cr	Zn	Ti
Debris side dry	0.0312	0.0055	0.0013	0.0051	0.0019	0.0029	0.0027
Debris side wet	0.0256	0.0028	0.0008	0.0042	0.0011	0.0014	0.0014
Debris	0.0092	0.0023	0.0020	0.0079	0.0005	0.0013	0.0004
Residue side dry	0.0357	0.0041	0.0010	0.0099	0.0013	0.0019	0.0026
Residue side wet	0.0216	0.0047	0.0008	0.0045	0.0011	0.0008	0.0013
Al 6061 Max	0.0073	0.0042	0.0016	0.0125	0.0037	0.0026	0.0016
Al 6061 Min	0.0000	0.0015	0.0000	0.0081	0.0004	0.0000	0.0000

4. DISCUSSION

To summarize the results of this assessment, aluminum corrosion product was present at both of the sites where residue was observed on the aluminum basket rails. The aluminum-rich material was amorphous, and had a morphology that suggests it formed as a gel. The material decrepitated under the electron beam, indicating that it still contained water. SEM/EDS and FTIR analysis indicate that material is likely to be hydrous aluminum hydroxide. SEM analysis showed that the spongy residue sample from one of the sites consisted largely of filamentous fungal material. At the "residue" site, this fungal mat coated most or all of the corroded region. Embedded within and on the fungal material were grains of the aluminum corrosion product. A brown coating was present on much of the aluminum hydroxide and on parts of the fungal mass. Originally suspected of being iron oxide, the brown coating instead appeared to be organic in nature. The coating was enriched in K, Fe, and P. However, these elements were largely disseminated, occurring as complexed species rather than discrete phases in the coating. Also present at each of the two corrosion sites were insect fragments; moreover, dead insects were observed via borescope at the bottom of the cask.

Chemical analysis of the samples collected from the residues showed that many trace metals were present, most of them in amounts consistent with their source being corrosion of Al-6061, the material comprising the basket rails. Elements present in greater amounts than could be explained by corrosion of the aluminum metal are K (the second most abundant metal in the samples), Fe, and P, the species enriched in the organic coating. The brown material is interpreted to consist of fungal exometabolites and breakdown products of the wood (e.g. organic acids); fungal exometabolites specifically scavenge important nutrients such as K, Fe, and P from the wood as it is broken down, making them bioavailable to the fungus. It is clear from the presence of these elements (which must be sourced to the wood), and the presence of the fungus and insect fragments, that the polypropylene wrapping on the cribbing was leaking or possibly damaged, allowing fluids from the wood to contact the aluminum metal.

There are a number of potential explanations for the observed attack on the aluminum basket rails:

- Crevice corrosion
- Corrosion due to chemicals used for wood treatment (a number of which are aggressive with respect to aluminum) leaching out of the cribbing.
- Corrosion due to organic acids leaching out of the wood.
- Corrosion due to alteration of the local chemistry by fungi.

Crevice corrosion requires an occluded geometry that sufficiently limits transport of electrolyte species (e.g., O₂, H⁺), setting up different environmental conditions between outside and inside the crevice (e.g., acidification in crevice and/or different metal ion concentrations) and/or causes sufficient potential drop (IR) for de-passivation to occur. Crevice corrosion of aluminum is unlikely in the absence of aggressive species, but in this case, possible aggressive species include organic compounds produced by leaching of organic acids from the wood and by fungal attack of the wood which clearly occurred. There is no evidence that anoxic conditions occurred developed in the corroded area. Fungi are aerobes, and the presence of the fungal matter, at the "debris" location, where the fungal mycelium covers most or all of the corroded site, suggests that

conditions were oxic. Could the fungi have infiltrated into the crevice and into the aluminum-rich gel after cessation of corrosion and the return of aerobic conditions, but prior to hardening of the gel? This is not consistent the observed texture of the "debris" sample, which clearly shows that gel formed on the surface of the existing fungal material; the fungal material is not embedded in the gel, as it would be if it had infiltrated an existing gel. Moreover, the morphology of the aluminum gel suggests that it formed by evaporation on a free surface, indicating that the top of the fungal mat was exposed to the air in the cask. Finally, aluminum is toxic to fungi, as it is to all living things, and infiltration of fungal mycelium into a concentrated aluminum gel is not rational. It is possible that crevice corrosion occurred elsewhere—in a region where the fungal mat was not present—and the aluminum diffused out of the crevice and solidified into a gel on the fungal mat; however, at the debris site, the fungal material appears to cover most or all of the corroded area. Given the presence of organic compounds and fungi that are known to support corrosion in oxic conditions, there is little reason to speculate that an anoxic crevice developed. Although the crevice may not have generally been anoxic, other chemical gradients, such as variation in pH, may have developed due to the occluded geometry that promoted crevice corrosion. It is also possible that the major role of the crevice, if present, was to trap water via capillary action, maintaining wet conditions against the aluminum metal.

Standard wood treatments to eliminate insect infestation and fungal rot include chromated copper arsenate (widely used for industrial applications) and several copper compounds, involving both organic copper compounds and sub-micron metallic copper (WWPI, 2011). These copper-bearing compounds are corrosive with respect to aluminum. However, in this case, fungi and possibly living insects were present, suggesting that the wood was not treated. Moreover, the wood treatments are quite concentrated, and in order to be effective, retention of the chemicals in the wood is required to be at levels of 0.1 to 0.4 lb/ft³ (WWPI, 2011) which, depending on wood density, equates to 0.3 to 1.8% by weight (thousands to tens of thousands of ppm). Other than nutrients extracted from the wood (Fe, K, and P), the metals present in the samples, including Cu, were not significantly elevated relative to what would be released from the aluminum alloy (ASTM-B-221-6061-T6) as it corroded, assuming stoichiometric dissolution, again suggesting that none of these wood treatments were used. An additional wood treatment that is commonly used in potassium borate; however, although elevated potassium was observed in the samples, boron (readily measured by ICP-MS) as not detected, indicating that this treatment was also not used. Thus, it is concluded that wood treatments were not responsible for the observed aluminum corrosion.

Organic acids leached from the wood are a possible cause of the observed corrosion, and this can occur in oxic conditions. It is well known that freshly-cut hardwoods and softwoods emit corrosive compounds, including acetic and formic acids and formaldehyde (Arni et al., 1965a; Arni et al., 1965b; Ryhl-Svendsen and Glastrup, 2002; Gibson and Watt, 2010). These compounds are generated both by chemical reactions and microbiological activity in the fresh wood (Arni et al., 1965a). The brown organic film observed at both sites is clearly sourced to degradation of the wood. However, given the presence of fungi that readily decompose wood for nutrients and the observed enrichment of nutrients (iron, phosphorous, and potassium) in the organic material at both the corroded sites, it is likely that fungi played a role in the corrosion. Wood degradation and production of organic acids are greatly increased by fungal activity (all common types of wood rot are fungal processes, Fungiora, 2006); moreover, fungi release exometabolites to aid in wood

breakdown and nutrient extraction. These exometabolites include siderophores, which include the strongest known complexants for Fe and other metals. For instance, for enterobactin, a bacterially-produced siderophore, the formation constant K for the Fe complex is $>10^{45}$ (Hider et al., 1981).

As discussed in Section 3.1, it is clear that fungal activity, and probably insect activity, occurred after the cribbing was placed in the cask and the cask sealed. The insects may have been wood beetles living in the wooden cribbing. Damage to the plastic that was wrapped around the cribbing, or simply gaps in the wrapping, allowed aqueous solutions from the infested regions to contact the aluminum and cause corrosion. In the case of the "debris location", the fungal mycelium itself extended through the plastic and coated the metal. One role of the fungus may have been to produce a wet biofilm and a moist environment on the aluminum surface. Fungal breakdown of wood produces water as a metabolic byproduct, and that water is retained in the moist biofilm surrounding the fungus, eliminating any need for excess moisture or condensation within the plastic wrap surrounding the cribbing.

However, it is more likely that the fungus played a more active role in the aluminum corrosion by (1) decomposing the wood and enhancing organic acid leach rates; and (2) producing corrosive exometabolites. Fungi decompose wood largely by use of enzymes that break down cellulose or lignin, although some also generate hydrogen peroxide. The fungi break down wood to produce organic compounds including a variety of organic acids that lower the pH in the biofilm (Hammel, 1997; Sánchez, 2009). The organic acids are also strong complexants of metal ions including iron and aluminum, increasing their solubility and potentially destabilizing the oxide layer on the aluminum. The fungus itself releases compounds called siderophores that strongly chelate metal ions and may have damaged the oxide layer on the aluminum. Fungi release siderophores to complex and solubilize iron, a necessary nutrient, making it more bioavailable. While iron is most strongly bound by siderophores, aluminum is also chelated (Roy and Chakrabartty, 2000; Rogers et al., 2001; Illmer and Buttinger, 2006). Increasing Al concentration as the pH drops due to organic acid production will probably stimulate a rise in siderophore production (although this has a complex dependence on the available Fe concentration). The reason for the increase in siderophore production is not well understood, but appears to be either in an effort to (1) chelate and detoxify Al; (2) increase iron availability by reducing the effects of Al-Fe competition for siderophores; or (3) simply in response to oxidative stress (Illmer and Buttinger, 2006). However, if elevated Fe is present, then siderophore production does not increase, as sufficient Fe is present in soluble form to support bioactivity regardless of the aluminum. In the case of the high-burnup cask, Fe concentrations were elevated—about 1-3% of the total Al values in the bulk sample (which is extremely high given the very low solubility of Fe oxides), and the Fe-to-soluble Al ratio was probably even higher, since Fe is preferentially complexed by siderophores. This may have limited fungal sensitivity to Al concentrations and allowed continued growth of the fungus, even after the aluminum began to corrode.

Corrosion of aluminum by fungi has previously been reported. Belov et al. (2008) performed an experimental study with aluminum coupons exposed to water containing fungal spores, both in the presence and absence of a growth medium. The results indicated that the fungi did not utilize aluminum directly as an energy source, but did cause aluminum to corrode in the presence of a growth medium. The cause of corrosion was not clear. Initially, an exudate of neutral to moderately basic pH formed on the surface of the aluminum, containing alkali metal ions that had

been extracted from the growth medium by the fungi. The formation of this moderately basic pH solution was attributed to the reaction of oxygen radicals produced by fungi with water to form hydroxyl ions and hydrogen peroxide. Over time, an aluminum-rich jelly-like material was formed; concomitantly, the pH dropped to neutral values. Initially, the corrosion product contained only aluminum species; however, over a few months, a significant fraction of the material was biogenic, consisting of a suite of organic acids. Belov et al. (2008) speculate that the organic acids actually form by cell lysis, after cell death; however, similar acids have been identified as metabolites produced by fungal breakdown of wood (Hammel, 1997; Sánchez, 2009). Acidic fungal metabolites and possibly, cellular lysis products have also been identified as facilitating localized corrosion of aluminum fuel tanks on aircraft (Salvarezza et al., 1983) (antifungal agents are frequently added to aircraft fuel specifically to avoid fungal corrosion of the aluminum tanks). Although chloride played a major role, the organic acids helped destabilized the protective oxide layer on the aluminum by lowing the pH of the medium, but also had an additional effect, possibly related to complexation of aluminum in solution.

Note that in the two studies above, wood was not present, and corrosion was attributed exometabolites produced by the fungi (e.g. oxygen radicals, siderophores), and possibly to products of cell lysis. The function of siderophores is to complex iron and increase its bioavailability, but these compounds are also strong ligands for Al. At the locations where corrosion was observed in the HBU demonstration cask, containing elevated levels of metal chelators probably damaged the protective oxide layer on the aluminum, resulting in corrosion. Later, after fungal death, organic acids produced by cell lysis and by degradation of the wood may have produced an acidic solution that further supported corrosion. This is consistent with the observed textural relationship in the "debris" sample, which indicates that the fungus preceded corrosion, and does not require that fungi have propagated in the aluminum-rich toxic gel that would have been produced by corrosion.

We speculate that the association of the fungi and insects in not coincidental, but rather that wood-boring beetles, which inoculate wood with fungi and then harvest the fungi for food, were present in the wood. While the presence of wood-boring beetles is speculative, it is noted that small dead insects were observed in the bottom of the cask during the inspection. When the cask is cleaned, the insects should be collected and identified to verify the hypothesis.

To summarize, several different possible corrosion mechanisms were considered. Corrosion due to wood treatments can be eliminated as a mechanism, because the distinctive chemical signature of such treatments was not found, and because such treatments are specifically intended to inhibit wood rot through fungal attack, and the presence of fungi shows that the wood was not treated. The presence of organic aggressor species in the seepage could have supported crevice corrosion, but evidence suggests that anoxic conditions did not occur. However, as noted previously, a crevice may have acted to capture water via capillary processes, keeping the contact area wet and allowing corrosion to occur. Moreover; a crevice was not necessary, because the organic compounds present would have corroded the metal in the absence of a crevice. These organic compounds include both organic acids leached from the wood—which would have been released in higher concentrations because of fungal degradation of the wood—and fungal exometabolites and products of cell lysis that complex Al and damage the passive layer on the metal surface. Given the evidence that the fungi preceded corrosion, and the presence of the fungi or organic

matter that clearly indicates fungal activity occurred at both corrosion sites, there is a strong likelihood that the fungi contributed to the corrosion; this is true whether of not the corrosion occurred in an anoxic crevice, or under oxic conditions. However, regardless of the mechanism, it is clear that corrosion of the aluminum metal was due to contact with the wooden cribbing.

5. CONCLUSIONS

On September 29-30, 2015, a team consisting of Electric Power Research Institute personnel, AREVA personnel (AREVA Federal Services, AREVA TN, and AREVA P&T), and personnel from Dominion Virginia Power performed an inspection of the TN-32B cask that will be used for the high-burnup demonstration project. During the survey, polypropylene-wrapped wooden cribbing that had been placed within the cask prior to shipment to prevent shifting of the basket was removed, revealing two small areas of residue on the aluminum basket rails, where they had contacted the cribbing. The nature of the residue was unknown, but it appeared to be a corrosion product and concerns were raised that similar attack could exist at more difficult-to-inspect locations in the canister. The decision was made to collect samples of the residue for evaluation and to allow a technical assessment of the observed attack.

Samples of the suspected corrosion residue were collected the next time the cask was opened (July, 2016) and sent to SNL for analysis. The materials consisted of a single bulk sample of the filamentous, spongy residue, and several samples collected by swiping the residues at each of the locations with 5-inch paper filters. At SNL, the samples were imaged and analyzed using a SEM/EDS. Bulk analysis was then carried out using ICP-MS.

Analysis of the samples showed that aluminum corrosion product was present at both sites. The aluminum-rich material was amorphous aluminum hydroxide, and formed as a gel. Filamentous fungal material was also present, as was brown organic material containing elevated levels of K, Fe, and P. Unidentifiable insect fragments were present at each of the two corrosion sites; moreover, dead insects were observed via borescope at the bottom of the cask. The presence of organic material enriched in these elements (which must be sourced to the wood), the fungus, and the insect fragments, indicates that the polypropylene wrapping on the cribbing was damaged, allowing fluids from the wood, or the wood itself, to contact the aluminum metal. It is clear that contact with the cribbing caused the observed corrosion.

The corrosion could have been due to a combination of crevice effects, organic acids leached from the wood, or fungal growth. Evidence suggests that fungal growth played an important role both through direct and indirect processes. Fungal activity produces powerful metal complexants that have been shown to promote aluminum corrosion, but also is the dominant mechanism of wood decay, increasing organic acid release. Regardless of the mechanism, it is clear that corrosion of the aluminum metal was due to contact with the wooden cribbing. Areas not contacted by the cribbing or fluids generated by it are unlikely to be corroded, and once the corroded sites and the cask interior have been thoroughly cleaned (the fluid may have dripped deeper into the cask), further corrosion over the course of the high-burnup demonstration test is unlikely. Regardless of the mechanism, it is clear that corrosion of the aluminum metal was due to contact with the wooden cribbing. Once the corroded sites and the cask interior have been thoroughly cleaned (the fluid may have dripped deeper into the cask), further corrosion over the course of the high-burnup demonstration test is unlikely.

6. REFERENCES

- Arni, P., Cochrane, G. and Gray, J. (1965a). The emission of corrosive vapours by wood. I. Survey of the acid-release properties of certain freshly felled hardwoods and softwoods. *Journal of applied chemistry* **15**, 305-313.
- Arni, P., Cochrane, G. and Gray, J. (1965b). The emission of corrosive vapours by wood. II. The analysis of the vapours emitted by certain freshly felled hardwoods and softwoods by gas chromato-graphy and spectrophotometry. *Journal of Chemical Technology and Biotechnology* **15**, 463-468.
- Belov, D., Sokolova, T., Smirnov, V., Kuzina, O., Kostyukova, L. and Kartashov, V. (2008). Corrosion of aluminum and its alloys under the effect of microscopic fungi. *Protection of Metals* **44**, 737-742.
- Fungiora, O. O. (2006). Wood and tree fungi: biology, damage, protection, and use. *Springer, BerlinStahli M, Finsinger W, Tinner W, Allgwer B* (2006) Wildfire history and re ecology of the Swiss National Park (Central Alps): new evidence from charcoal, pollen and plant macrofossils. Holocene **16**, 805817.
- Gibson, L. and Watt, C. (2010). Acetic and formic acids emitted from wood samples and their effect on selected materials in museum environments. *Corrosion Science* **52**, 172-178.
- Hammel, K. (1997). Fungal degradation of lignin. *Driven by nature: plant litter quality and decomposition. CAB International, Wallingford*, 33-46.
- Hider, R. C., Mohd-Nor, A. R., Silver, J., Morrison, I. E. and Rees, L. V. (1981). Model compounds for microbial iron-transport compounds. Part 1. Solution chemistry and Mössbauer study of iron (II) and iron (III) complexes from phenolic and catecholic systems. *Journal of the Chemical Society, Dalton Transactions*, 609-622.
- Illmer, P. and Buttinger, R. (2006). Interactions between iron availability, aluminium toxicity and fungal siderophores. *Biometals* **19**, 367-377.
- Lee, S. K., Lee, S. B., Park, S. Y., Yi, Y. S. and Ahn, C. W. (2009). Structure of amorphous aluminum oxide. *Physical Review Letters* **103**, 095501.
- Licht, H. H. D. F. and Biedermann, P. H. (2012). Patterns of functional enzyme activity in fungus farming ambrosia beetles. *Frontiers in zoology* **9**, 1.
- Rogers, N. J., Carson, K. C., Glenn, A. R., Dilworth, M. J., Hughes, M. N. and Poole, R. K. (2001). Alleviation of aluminum toxicity to Rhizobium leguminosarum bv. viciae by the hydroxamate siderophore vicibactin. *Biometals* **14**, 59-66.
- Roy, N. and Chakrabartty, P. K. (2000). Effect of aluminum on the production of siderophore by Rhizobium sp.(Cicer arietinum). *Current microbiology* **41**, 5-10.
- Ryhl-Svendsen, M. and Glastrup, J. (2002). Acetic acid and formic acid concentrations in the museum environment measured by SPME-GC/MS. *Atmospheric Environment* **36**, 3909-3916.
- Salvarezza, R., De Mele, M. and Videla, H. (1983). Mechanisms of the microbial corrosion of aluminum alloys. *Corrosion* **39**, 26-32.

Sánchez, C. (2009). Lignocellulosic residues: biodegradation and bioconversion by fungi. *Biotechnology advances* **27**, 185-194.

Vega, F. E. and Blackwell, M. (2005). *Insect-fungal associations: ecology and evolution*: Oxford University Press.

WWPI. (2011). Guide to Pressure Treated Wood. Western Wood Preservers Institute, 13 p.

Distribution

1 Keith Waldrop
Used Fuel and HLW Management Program
Electric Power Research Institute
1300 West WT Harris Blvd.
Charlotte, NC 28262

1 Ned Larson (electronic copy)
M/S NSF 165, Room B119
U.S. Department of Energy
232 Energy Way
North Las Vegas, NV 89030

1	MS0115	OFA/NFE Agreements	10012
1	MS0736	P. Swift	6220 (electronic copy)
1	MS0747	K. Sorenson	6223 (electronic copy)
1	MS0779	S. Saltzstein	6225 (electronic copy)
1	MS0899	Technical Library	9536 (electronic copy)

